Language Understanding for Field and Service Robots in a Priori Unknown Environments

Matthew R. Walter[1*] Siddharth Patki[2] Andrea F. Daniele[1] Ethan Fahnestock[2]
Felix Duvallet[3] Sachithra Hemachandra[4] Jean Oh[5] Anthony Stentz[5]
Nicholas Roy[6] and Thomas M. Howard[2]

[1]Toyota Technological Institute at Chicago
[2]University of Rochester
[3]Kodiak Robotics, Inc.
[4]Cruise
[5]Carnegie Mellon University
[6]Massachusetts Institute of Technology

Abstract

Contemporary approaches to perception, planning, estimation, and control have allowed robots to operate robustly as our remote surrogates in uncertain, unstructured environments. This progress now creates an opportunity for robots to operate not only in isolation, but also with and alongside humans in our complex environments. Realizing this opportunity requires an efficient and flexible medium through which humans can communicate with collaborative robots. Natural language provides one such medium, and through significant progress in statistical methods for natural-language understanding, robots are now able to interpret a diverse array of free-form navigation, manipulation, and mobile-manipulation commands. However, most contemporary approaches require a detailed, prior spatial-semantic map of the robot's environment that models the space of possible referents of an utterance. Consequently, these methods fail when robots are deployed in new, previously unknown, or partially-observed environments, particularly when mental models of the environment differ between the human operator and the robot. This paper provides a comprehensive description of a novel learning framework that allows field and service robots to interpret and correctly execute natural-language instructions in a priori unknown, unstructured environments. Integral to our approach is its use of language as a "sensor"—inferring spatial, topological, and semantic information implicit in natural-language utterances and then exploiting this information to learn a distribution over a latent environment model. We incorporate this distribution in a probabilistic, language grounding model and infer a distribution over a symbolic representation of the robot's action space, consistent with the utterance. We use imitation learning to identify a belief-space policy that reasons over the environment and behavior distributions. We evaluate our framework through a variety of different navigation and mobile-manipulation experiments involving an unmanned ground vehicle, a robotic wheelchair, and a mobile manipulator, demonstrating that the algorithm can follow natural-language instructions without prior knowledge of the environment.

1 Introduction

Advancements in perception, planning, and control have enabled robots to move from controlled isolation in factories and laboratories to semi-structured and unstructured environments. Notable domains where field and service robots have proven successful at operating in the presence of uncertainty include material handling (Durrant-Whyte, 1996; Durrant-Whyte et al., 2007; Walter et al., 2015), underground mining (Scheding et al., 1997, 1999; Roberts et al., 2000; Marshall et al., 2008; Duff et al., 2003), disaster mitigation (Nagatani

*Corresponding author: mwalter@ttic.edu

et al., 2008, 2013; Keiji et al., 2011), space science and exploration (Maimone et al., 2007; Furgale and Barfoot, 2010; Arvidson et al., 2010), underwater science and exploration (Singh et al., 2004; Johnson-Roberson et al., 2010; Williams et al., 2012; Yoerger et al., 2007; Bowen et al., 2008; Camilli et al., 2010; German et al., 2008), and autonomous driving (Thrun et al., 2006; Urmson et al., 2006, 2008; Bacha et al., 2008; Miller et al., 2008; Montemerlo et al., 2008; Bohren et al., 2008; Leonard et al., 2008). With few exceptions (Walter et al., 2015), however, current operational, field-robotic systems function with either full autonomy or under at least partially-supervised teleoperation. More common in field operations, including those conducted by the military (Kang et al., 2003; Ryu et al., 2004; Yamauchi, 2004), teleoperation places significant cognitive load on the operator, who must interpret the robot's multiple, diverse sensor streams in order to establish situational awareness, while simultaneously and continuously controlling the robot's low-level degrees of freedom. Consequently, teleoperation limits the effectiveness and efficiency of the tasks that can be performed.

A long-standing goal is to realize field and service robots that operate in the continuum between full autonomy and supervised teleoperation, not only as our surrogates, but also as our *partners* working with and alongside people. Achieving this goal requires command and control mechanisms that are both intuitive and efficient, and spoken language offers a flexible medium through which people can communicate with robots, without the need for specialized interfaces or significant training. For example, people can issue verbal instructions that direct robotic forklifts (Walter et al., 2015) to load and unload cargo in semi-structured storage and distribution facilities. Similarly, a voice-commandable wheelchair (Hemachandra et al., 2011) enables people with limited mobility to navigate their environments independently and safely simply by speaking to their wheelchair, rather than requiring the use of traditional sip-and-puff arrays or head-actuated switches.

Figure 1: A robot is directed to "retrieve the ball inside the box" in an a priori unknown environment.

The potential of natural language as an effective command and control mechanism has motivated significant advances in statistical approaches to language understanding. These models and algorithms enable robots operating in a variety of domains to interpret free-form instructions commanding tasks that include navigation (Kollar et al., 2010; Matuszek et al., 2010; Chen and Mooney, 2011; Matuszek et al., 2012; Thomason et al., 2015) and object manipulation (Tellex et al., 2011; Howard et al., 2014b; Thomason et al., 2016, 2018; Shridhar and Hsu, 2018), as well as to generate natural-language utterances (Tellex et al., 2014; Daniele et al., 2017; Shridhar and Hsu, 2018). Natural-language understanding is often formulated as a symbol-grounding problem, wherein the task is to associate linguistic phrases with their corresponding referents in the robot's symbolic model of its state and action spaces. Most contemporary approaches assume that this model is known a priori in the form of a "world model" that expresses relevant information about the robot's environment (e.g., the location, semantic class, and colloquial name of every object and spatial region that the user may refer to). Such a world model is typically constructed by manually adding semantic information to spatial maps produced using an off-the-shelf SLAM algorithm (Kaess et al., 2008, 2009). This practice inherently prevents natural-language understanding in environments that are unknown or partially known to the robot. Consider a mobile manipulator that is placed in a new environment consisting of multiple boxes that are all outside the field-of-view of the robot's sensors (Fig. 1). Suppose that a person directs the robot to "retrieve the ball inside the box". Without knowledge of the environment, the robot is unable to associate the phrases "the ball" or "the box" to specific locations (i.e., symbol instantiations). In this case, most existing methods would either fail to ground the instruction or cause the robot to naively explore the environment until it happens upon a ball contained in a box.

This paper provides a comprehensive presentation of a framework that enables robots to follow natural-language instructions that command navigation and mobile manipulation in a priori unknown environments (Fig. 2). Key to our approach is its exploitation of the spatial, topologic, and semantic information that the utterance conveys, effectively treating language as another "sensor." Three algorithmic contributions are

integral to this formulation.

- First, a learned language-grounding model efficiently infers environment "observations," implicit or explicit in the command, as well as the desired behaviors.
- Second, an estimation-theoretic algorithm hypothesizes the structure of the unobserved environment by using these language-based observations and those from the robot's traditional sensor streams to build and maintain a probability distribution over the world model (Fig. 2(b)).
- Third, an imitation learning-based approach learns a belief-space policy that reasons over this world model distribution to identify navigation and manipulation actions that are optimal, given limited environment knowledge (Fig. 2(d)).

In the following sections we first position our work in the context of contemporary approaches to language understanding. We then provide a thorough technical description of the proposed model and give the details of the experimental results on navigation and mobile manipulation tasks using three different robotic platforms. We then conclude with a discussion of the strengths and weaknesses of the proposed approach, along with directions for current and future work that seeks to address these limitations in order to facilitate more efficient human-robot collaboration.

2 Related Work

Natural-language understanding for human-robot interaction has been studied extensively over the past several decades. Symbol grounding (Harnad, 1990) is a common approach to language understanding, whereby words and phrases are interpreted in terms of their associated symbols in the robot's model of the world. Early work in symbol grounding (Winograd, 1971; Roy et al., 2003; MacMahon et al., 2006) utilizes manually engineered correspondences and features that relate words to symbols comprised of the actions and a structured environment model. Consequently, these approaches employ a compact, predetermined grammar and a small set of symbols that limit the diversity of language that they can handle.

In contrast, contemporary approaches use statistical models that are trained in a data-driven fashion to learn to express a large set of linguistic, spatial, and semantic features. These approaches enable robots to successfully interpret natural-language utterances that command navigation (Kollar et al., 2010; Matuszek et al., 2010; Chen and Mooney, 2011; Matuszek et al., 2012; Thomason et al., 2015), object manipulation (Bollini et al., 2010; Howard et al., 2014b; Misra et al., 2016; Thomason et al., 2016, 2018; Shridhar and Hsu, 2018; Paul et al., 2018), and mobile manipulation (Tellex et al., 2011; Walter et al., 2015), as well as to generate natural-language utterances (Tellex et al., 2014; Daniele et al., 2017; Shridhar and Hsu, 2018) in a variety of complex domains. Data-driven approaches to symbol grounding (Tellex et al., 2011; Howard et al., 2014b,a; Paul et al., 2018) learn probabilistic models that exploit the hierarchical structure of language in order to associate (i.e., "ground") each phrase in an utterance to its corresponding referent in a symbolic representation of the robot's state and action spaces. These methods generally require that the robot has prior knowledge of the the environment, for example in the form of a spatial-semantic map of the different objects and regions (e.g., rooms). In practice, these maps are often generated by first teleoperating the robot around the environment and using a state-of-the-art SLAM algorithm (Olson et al., 2006; Kaess et al., 2008) to build a metric map of the environment. These maps are then manually annotated to include semantic information, e.g., by delineating each object and room, and then assigning them a label, to arrive at an environment map sufficient to provide a symbolic world model. An alternative is to incorporate this information as part of the initial mapping using a semantic SLAM framework (Galindo et al., 2005; Martínez Mozos et al., 2007; Meger et al., 2008; Vasudevan and Siegwart, 2008; Krieg-Brückher et al., 2005; Zender et al., 2008; Pronobis et al., 2010; Hemachandra et al., 2011; Pronobis and Jensfelt, 2012). These approaches build on the effectiveness of SLAM by augmenting a low-level metric map with layers that encode the topological and semantic properties of the environment extracted from the robot's sensor data (e.g., LIDAR scans and camera images), using scene classifiers (Nüchter et al., 2003; Martínez Mozos et al., 2007; Pronobis et al., 2010) and object detectors (Torralba et al., 2003; Meger et al., 2008; Vasudevan and Siegwart, 2008; Kollar and Roy, 2009). For a comprehensive discussion of the role of environment representations in language-based spatial reasoning, we refer the reader to the survey by Landsiedel et al. (2017).

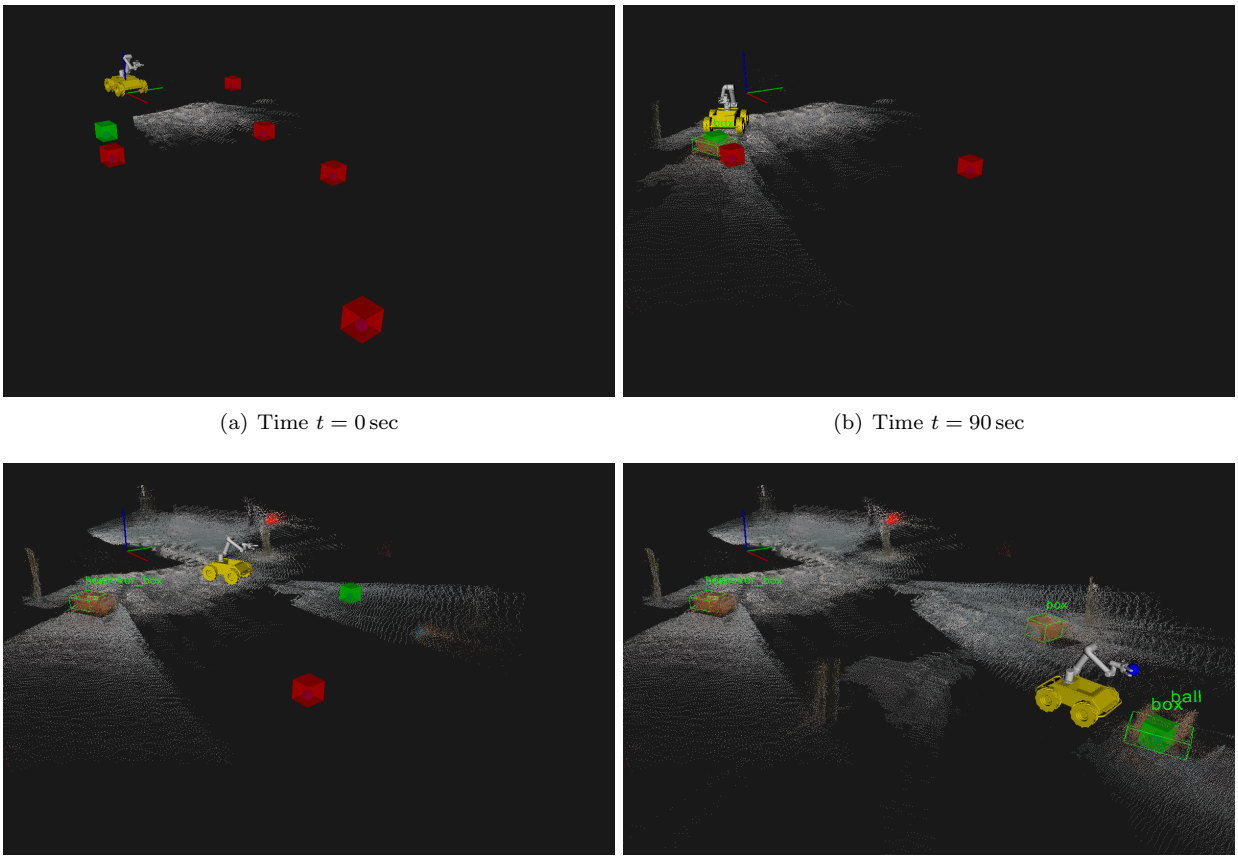

(a) Time $t = 0\,\text{sec}$

(b) Time $t = 90\,\text{sec}$

(c) Time $t = 320\,\text{sec}$

(d) Time $t = 563\,\text{sec}$

Figure 2: Our framework learns to exploit environment-related information implicit in a given utterance to hypothesize a distribution over possible maps in a priori unknown environments. Traditional approaches to language grounding involve reasoning over a detailed world model that is assumed to be known a priori. In order to allow grounding in a priori unknown or partially observed environments, our method maintains a distribution over hypothesized, spatial-semantic maps based upon environment information conveyed in the utterance. Consider a scenario in which the robot is instructed to "pick up the ball inside the box" in an unknown environment. Upon receiving the instruction, (a) the algorithm uses information extracted from the command to hypothesize the location of potential boxes, some of which contain a ball. Here, we visualize samples drawn from this distribution. The solid green cube denotes the hypothesized box that is the current goal of the planner. As the robot navigates, it (b) detects actual boxes (green wireframe) that are found to not contain a ball, while also failing to confirm the presence of hypothesized boxes sampled from the distribution. The algorithm updates the world model distribution accordingly, and the planner updates the goal. This continues until (d) the robot observes a box containing a ball and subsequently retrieves the ball, satisfying the instruction.

While most language grounding methods rely on access to such a prior map of the environment, there are notable exceptions that are capable of language understanding in unknown environments. Particularly relevant is the work of Duvallet et al. (2013), which opportunistically builds a deterministic map of the a priori unknown environment as the robot navigates. This map serves as input to a policy that is trained via imitation learning to emulate the way in which humans follow instructions in unknown environments. Our approach similarly uses imitation learning to identify the robot's policy based on human demonstrations, but unlike the work of Duvallet et al. (2013), our policy reasons over a probabilistic model of the environment that makes explicit information that the instruction conveys. Also relevant are recent neural network-based approaches to language-based navigation in novel (i.e., unknown) environments (Mei et al., 2016;

Anderson et al., 2018). Unlike our approach, these methods map language directly to actions, and do not (explicitly) infer a distribution over possible world models from language. Meanwhile, statistical parsing-based methods (Matuszek et al., 2010; Chen and Mooney, 2011; Matuszek et al., 2012; Thomason et al., 2015) associate natural-language utterances to a meaning representation that typically takes the form of a lambda calculus. Such an approach avoids the need for an explicit world model, typically at the expense of requiring a down-stream controller capable of executing inferred plans in unknown environments.

Also relevant is recent work that focuses on grounding unknown or ambiguous utterances. One approach to dealing with ambiguous utterances is to utilize inverse grounding (Tellex et al., 2014; Gong and Zhang, 2018) to generate targeted questions for the user that are deemed to be most informative, e.g., in terms of the reduction in entropy for the grounding distribution (Tellex et al., 2012). Meanwhile, several methods learn a priori unknown grounding models by exploring the relationship between novel linguistic predicates and the robot's world model and/or its percepts (Thomason et al., 2016; She and Chai, 2017; Tucker et al., 2017; Thomason et al., 2018). Our work differs in that we assume that the concepts are known, but that the instantiations of these concepts in the robot's environment are unknown.

Meanwhile, much attention of late has been applied to the problem of navigating a priori unknown environments towards a desired goal using only onboard sensing, typically in the form of monocular or RGBD images (Kim and Chen, 2015; Zhu et al., 2017; Gupta et al., 2017; Rasouli et al., 2020), laser scans (Chiang et al., 2019; Zeng et al., 2019), or a combination of the two (Kollar and Roy, 2009; Aydemir et al., 2011, 2013). While language typically plays little-to-no role in these approaches (e.g., the goal may be specified by its named type), they are relevant to our work in that they learn a policy that is responsible for deciding where to navigate to next based on the robot's observation history. Similar to our approach, earlier work in this area reasons over a structured state space that is assumed to be partially observable. Search is then formulated as a decision-theoretic problem (e.g., in the context of a POMDP), whereby methods attempt to solve for the policy that is optimal based on the current state distribution. Similar to the way in which we use language to inform this distribution, these active search methods may exploit object-object and object-scene co-occurrence information (Kollar and Roy, 2009), spatial relations (Aydemir et al., 2011), or scene semantics (Aydemir et al., 2013).

Most recent approaches to active visual search model the navigation policy as a neural network that maps low-level sensor data directly to actions. Trained in an end-to-end manner via reinforcement learning, the architectures learn to reason over scene semantics in an entirely data-driven fashion. In contrast, our framework maintains a distribution over the seen and unseen parts of the world, which serves as an explicit, intermediate representation suitable for language grounding and planning under uncertainty. Another notable difference compared to our work is that this family of methods typically assumes that the agent is aware of the distance and direction of the goal (i.e., the location of the goal relative to the robot) at each time step. In practice, this means that there is some way of localizing the robot in the environment (presumably, using an a priori map available to an oracle). We assume that the robot has no such information. Additionally, they assume that the agent's motion and observations are noise-free, which is not true for robots in practice. With few exceptions (Sadeghi and Levine, 2017; Tai et al., 2017; Bansal et al., 2019), these methods have thus only been demonstrated in photorealistic simulators or on datasets (Mirowski et al., 2018; Zeng et al., 2019).

A key aspect of our approach is its use of language as a sensor, whereby information conveyed in the instruction is used to build and maintain a distribution over the map of the environment. In this way, our approach is similar to recent methods that enable robots to learn spatial-semantic environment models from linguistic descriptions together with traditional sensor streams (Zender et al., 2008; Pronobis and Jensfelt, 2012; Walter et al., 2013, 2014; Hemachandra et al., 2014). Our method builds on this work in order to maintain a distribution over a model of the environment. However, this earlier work assumes access to free-form utterances that explicitly describe the robot's environment. In contrast, our proposed framework learns to infer environment knowledge that is implicit in natural-language descriptions. Additionally, these previous approaches focus on estimation as it pertains to building spatial-semantic environment models, whereas we consider mapping jointly with planning under uncertainty specifically to satisfy a user's natural-language instruction.

3 Technical Approach

Contemporary approaches to natural-language understanding formulate the problem as probabilistic inference over a learned distribution that associates linguistic elements with their corresponding referents in a symbolic representation of the robot's state and action spaces. The space of symbols $\Gamma = \{\gamma_1, \gamma_2, \ldots, \gamma_n\}$ includes concepts derived from the robot's environment model, such as the location and category of objects and spatially extended regions (e.g., rooms, buildings, etc.), and a symbolic representation of viable robot behaviors, such as manipulating a specific object or navigating to a desired location. The distribution over symbols is conditioned on the parse of the free-form utterance $\Lambda_t = \{\lambda_1, \lambda_2 ... \lambda_n\}$,[1] and a world model S_t that represents environment knowledge extracted from the history of sensor measurements z^t using a set of perceptual classifiers. Framed as a symbol-grounding problem (Harnad, 1990), natural-language understanding then typically follows as maximum a posteriori inference over the power set of referent symbols $\mathcal{P}(\Gamma)$

$$\Gamma_t^* = \arg\max_{\mathcal{P}(\Gamma)} p(\Gamma | \Lambda_t, S_t). \tag{1}$$

This approach reasons over a model of the world S_t that is assumed both to be known a priori and to express all information necessary to ground the given utterance. This precludes language understanding in unobserved (i.e., novel) or partially observed environments for which the world model is empty or incomplete, making accurate inference (1) infeasible.

3.1 Approach Overview

We address this problem by treating symbol grounding as inference conditioned on a *latent* model of the robot's environment S_t. In particular, we learn a probabilistic world model that exploits environmental information implicit in an utterance to build and maintain a distribution over the topological, metric, and semantic properties of the environment

$$p(S_t | \Lambda^t, z^t, u^t), \tag{2}$$

where Λ^t, z^t, and u^t denote the history of utterances, sensor observations (e.g., laser scans, image streams, and object detections from the robot's perception pipeline), and odometry, respectively. In this way, we maintain a world model distribution that not only fuses information perceived with sensors onboard the robot, but also models the unperceived information about the environment that is expressed in the utterance. Treating the environment model as a latent random variable, we formulate symbol grounding as a problem of inferring a distribution over robot behaviors β_t. A behavior in β_t is a symbolic representation of the intended robot actions expressed by the symbols in the inferred groundings Γ_t^*, and may include navigating to a specific location, grasping a particular object, etc.

The optimal trajectory x_t^* that the robot should take in the context of a distribution over behaviors then amounts to a planning under uncertainty problem formulated as inference over a model that marginalizes over the space of world models and robot behaviors

$$x_t^* = \arg\max_{x_t \in X_t} \int_{S_t} \int_{\beta_t} \underbrace{p(x_t | \beta_t, S_t)}_{\text{planning}} \times \underbrace{p(\beta_t | \Lambda_t, S_t)}_{\substack{\text{behavior} \\ \text{inference}}} \times \underbrace{p(S_t | \Lambda^t, z^t, u^t)}_{\substack{\text{semantic} \\ \text{mapping}}} dS_t \, d\beta_t \tag{3}$$

By structuring the problem in this way, we approach language understanding in a priori unknown environments as inference over three coupled learning problems. The framework (Fig. 3) first converts the parsed natural-language instruction into a set of environment annotations using a learned language grounding model. It then treats these annotations as observations of the environment (i.e., the existence, name, and relative location of objects and rooms) that it uses together with data from the robot's onboard sensors to learn a distribution over possible world models (the third term in Eqn. 3). Following the example of executing the command to "retrieve the ball inside the box" (Fig. 1), this may result in a distribution that hypothesizes the potential location of boxes in the environment, some of which contain hypothesized balls (Fig. 2(a)). Our framework then infers a distribution over behaviors conditioned on the world models and the current utterance (the second term in Eqn. 3). In our example, this distribution would favor performing

[1] In this way, we assume that the instructions are grammatically correct.

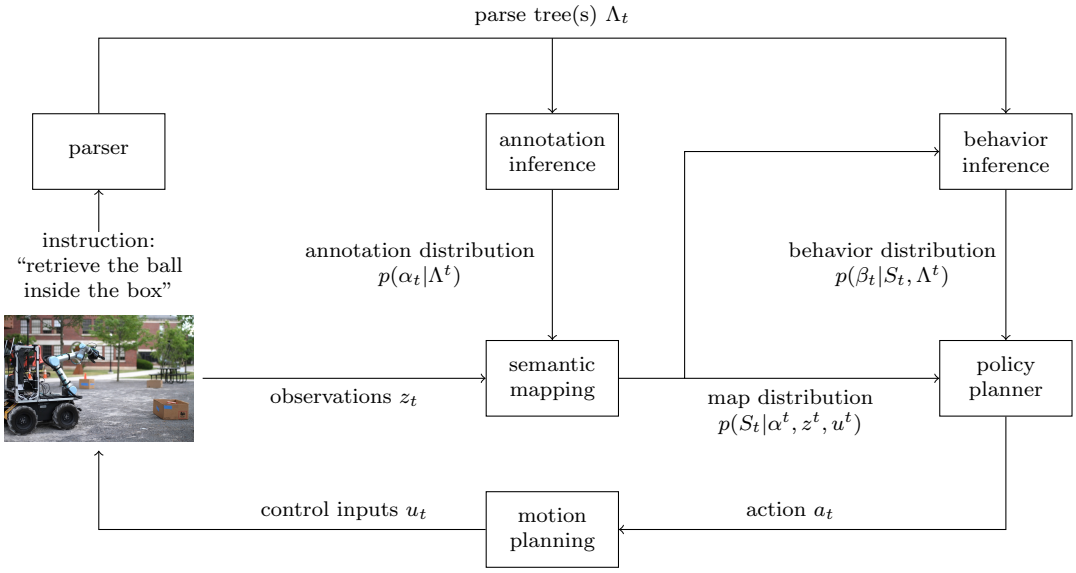

Figure 3: Our framework for language understanding in a priori unknown environments exploits environment descriptions available in a given instruction together with traditional sensing modalities to maintain a distribution over the environment model. A policy then reasons over this distribution together with inferred behaviors to identify an appropriate high-level action (e.g., an intermediate goal). A motion planner converts these actions into control inputs that the robot executes. This process then repeats as the robot makes new observations, until the policy decides that the instruction has been satisfied. Details regarding state estimation, semantic perception, etc. are omitted for clarity.

the "pick" action on an object of type "ball" whose location is consistent with being "inside" a box. Note that we assume that relevant information in any previous utterances, i.e., Λ^{t-1}, is captured in the map distribution. We then solve for the navigation and/or manipulation actions that are consistent with this behavior distribution (the first term in Eqn. 3) using a learned belief-space policy that commands a single, high-level action to the robot (e.g., navigating to a location where there is a high likelihood of there being a box). As the robot executes this action, we update the world model distribution based upon any new utterances and sensor observations, and subsequently select an updated action according to the policy. This process repeats until the policy concludes that the robot satisfied the instruction.

Reasoning over the entire space of behaviors and semantic maps would be intractable, particularly as the environment and behavior spaces grow. In order to make instruction-following tractable, we employ approximations to the individual distributions in Equation 3 as well as use approximate inference methods. In particular, we represent the latent map and behaviors as discrete samples from their respective distributions. Each map sample represents one hypothesis of the robot's environment, and each behavior sample is a set of action constraints inferred from language in the context of a particular hypothesized map. We maintain the world model distribution using a Rao-Blackwellized particle filtering framework. The following details each component of our approach.

3.2 Natural-Language Understanding

The approach to natural-language understanding of robot instructions in this paper relies on variations of the Distributed Correspondence Graph (DCG) (Howard et al., 2014b; Hemachandra et al., 2015; Boteanu et al., 2016; Barber et al., 2016; Broad et al., 2017; Oh et al., 2017; Patki and Howard, 2018; Arkin et al., 2018; Patki et al., 2019; Arkin et al., 2020). The DCG and the Hierarchical Distributed Correspondence Graph (HDCG) (Chung et al., 2015), Adaptive Distributed Correspondence Graph (ADCG) (Paul et al., 2016), and Hierarchical Adaptive Distributed Correspondence Graph (HADCG) (Paul et al., 2018) variations of the model formulate the problem of natural-language understanding as probabilistic inference in a factor graph

using models to approximate the conditional probabilities of a correspondence variable ϕ in the context of language Λ, symbols Γ, and the environment model S from corpora of annotated examples. Such models have the ability to generalize to instructions that are not explicitly represented in the corpora by independently learning the conditional probabilities of concepts for linguistic structures like nouns (e.g., "the box" and " briefcase"), prepositions (e.g., "near" and "inside"), and verbs (e.g., "drive" and "pick up") and leveraging the structure of the parse tree for probabilistic inference. Natural-language instructions are converted to parse tree representations to construct DCGs in this framework as studied and more explicitly demonstrated in Paul et al. (2018). Inference is made efficient by assuming conditional independence across linguistic and symbolic constituents. The HDCG, ADCG, and HADCG employ approximations of the symbolic representation Γ informed by expressed symbols to further improve the efficiency of probabilistic inference. Consider the example illustrated in Figure 4. This figure shows the DCG and the corresponding parse tree for the instruction "retrieve the ball inside the box". Each of the symbols γ_{i_j} in this graph represent objects, spatial relations, actions, and other concepts needed to interpret the meaning of the instruction. The connection to the environment model S is implicit in this illustration of the DCG.

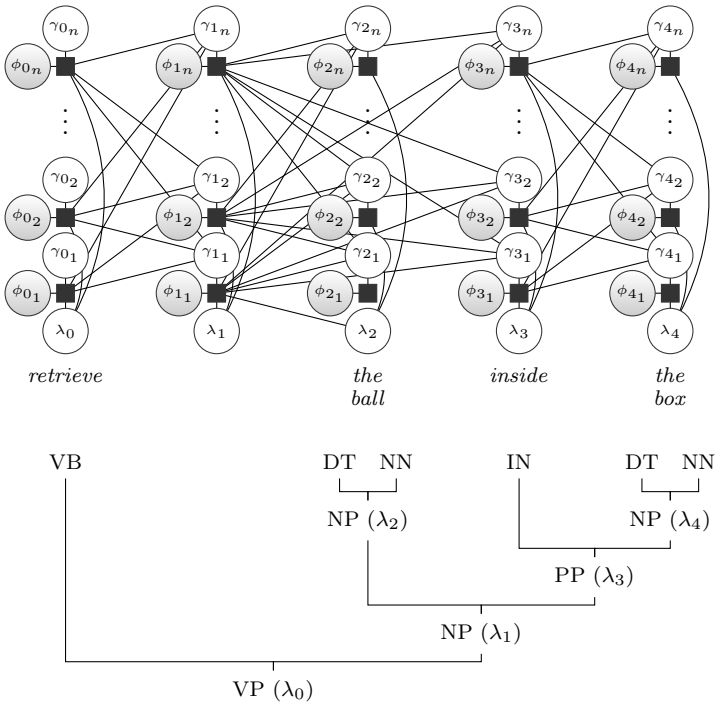

Figure 4: The DCG for the expression "retrieve the ball inside the box" aligned with the corresponding parse tree. The observed and unknown variable nodes in the factor graph are shown in white and gray, respectively.

Assuming that the symbol-grounding model is accurately trained from corpora of annotated examples, there are three potential outcomes that are observed to be conditioned on the information contained in the robot's model of the environment. To illustrate such outcomes, we consider the example utterance "the ball inside the box" from Figure 1. First, if the environment model is known or partially known and there is only one "ball" object that is uniquely identified as being inside of a "box" object, then the inference procedure returns a behavior that describes the navigation and manipulation action with respect to those physically grounded objects. Second, if the environment model is known or partially known and there is more than one "ball" object that satisfies the relationship of being inside of a "box" object, then the model would express this ambiguity to the user through a different set of symbols. The third case, which is the focus of this paper, is that the environment model is partially known and there are no "ball" objects that satisfy the relationship of being inside of a "box" object. The results of the inference procedure are no symbols that express a relationship to this unknown object because the object and the corresponding

actions and spatial relations are not part of the symbolic representation Γ. However, the user implies that there is an object that satisfies a specific relationship, indicating that their representation of the world is richer in this dimension than the robot's environment model. We therefore approach the problem of natural-language understanding as a two-part process that first exploits the environment-related information explicit or implicit in the utterance to build a distribution over possible world models that now contains hypothesized objects and spatial relationships that were missing in the incomplete world model. This is followed by a step that infers the behaviors in the context of this distribution over environment models that is informed by sensor observations and the information gleaned from the first step. The first and second steps, described as annotation inference and behavior inference, respectively, use specially adapted symbolic representations suitable for each problem. We describe the space of symbols in the annotation and behavior inference models as in Paul et al. (2018), which expresses each space as the union of different symbols and their constituents.

For annotation inference, we assume a symbolic representation that is independent of an environment model because it is meant to inform the state of the world, whereas behavior inference exploits the synthesized environment model from the semantic mapping process using the outputs of annotation inference and past sensor observations. The symbolic representation for annotation inference is defined by four different types of symbols. First, a space of object classes $\Gamma^{\mathcal{O}_\mathcal{C}}$ is defined by an object type $\mathcal{O}_\mathcal{C}$. These symbols represent the meaning of noun phrases like "box" or "ball" in the aforementioned example. Note that object class symbols do not correspond to specific instances of these objects in the environment model. Object class symbols bridge the gap between the diversity of language and the space of semantic object classes interpretative by the robot. Second, a space of locations $\Gamma^{\mathcal{L}}$ corresponds to physical locations in the environment model defined by a location type $\mathcal{L}$. These are similar to objects in that they occupy some bounded region in the environment model, but they are not observed using traditional object detectors to infer their location. Third, a space of spatial relation classes $\Gamma^{\mathcal{S}}$ is defined by a spatial relation label $\mathcal{S}$. Spatial relation classes can be used to represent noun phrases like "the left" or "front". Next, we define a space of region types $\Gamma^{\mathcal{R}_\mathcal{S}}$ by a spatial relationship class $\mathcal{S}$ for every object class in $\mathcal{O}_\mathcal{C}$. Region classes are used to represent prepositional phrases like "inside the box" or "to the left of the ball'. Lastly, a space of relationships $\Gamma^{\mathcal{R}_\mathcal{C}}$ is defined by a spatial relationship $\mathcal{S}$ between a pair of object classes in $\mathcal{O}_\mathcal{C}$. Relationship classes are used to represent spatial relationships between pairs of objects that occur in noun phrases like "the ball inside the box" or "the car behind the garage". When environments are partially observed, the extraction of these relationships from language can inform the distribution of objects and locations in the environment model constructed from visual perception. These relationships can be extracted implicitly from instructions like "pick up the ball from inside the box," or the last of part of a dialogue that begins with an ambiguous instruction (e.g., "pick up the ball" in an environment without a ball), a question that the robot poses to the human ("where is the ball"), and a response describing one or more of these relationship ("the ball is inside the box underneath the table on the far side of the room"). The space of symbols for annotation inference $\Gamma^{\mathcal{A}}$ is defined as the union of object, spatial relation, region, and relation symbols

$$\Gamma^A = \left\{\Gamma^{\mathcal{O}_\mathcal{C}} \cup \Gamma^{\mathcal{L}} \cup \Gamma^{\mathcal{S}} \cup \Gamma^{\mathcal{R}_\mathcal{S}} \cup \Gamma^{\mathcal{R}_\mathcal{C}}\right\}, \tag{4a}$$

where the constituent symbol spaces are defined as

$$\Gamma^{\mathcal{O}_\mathcal{C}} = \left\{\gamma_{o_{c_i}} | o_{c_i} \in \mathcal{O}_\mathcal{C}\right\} \tag{4b}$$

$$\Gamma^{\mathcal{L}} = \{\gamma_{l_i} | l_i \in \mathcal{L}\} \tag{4c}$$

$$\Gamma^{\mathcal{S}} = \{s_i | s_i \in \mathcal{S}\} \tag{4d}$$

$$\Gamma^{\mathcal{R}_\mathcal{S}} = \left\{\gamma^{s_i}_{o_{c_j}} | s_i \in \mathcal{S}, o_{c_j} \in \mathcal{O}_\mathcal{C}\right\} \tag{4e}$$

$$\Gamma^{\mathcal{R}_\mathcal{C}} = \left\{\gamma^{s_i}_{o_{c_j}, o_{c_k}} | s_i \in \mathcal{S}, o_{c_j} \in \mathcal{O}_\mathcal{C}, o_{c_k} \in \mathcal{O}_\mathcal{C}\right\}. \tag{4f}$$

For behavior inference, we assume a symbolic representation formed from objects, spatial relations, and regions. The space of objects $\Gamma^{\mathcal{O}}$ is described by the object $\mathcal{O}$ from the environment model S. These symbols represent actual objects that the robot has a model of and enables unique reference of objects by their semantic class ("the box" in an environment model with only one box) or by their spatial, temporal, or other relationship to other objects in an environment not uniquely defined by their semantic class ("the

box underneath the table" in an environment with several boxes but only one table or bench). The space of regions $\Gamma^{\mathcal{R}_\mathcal{O}}$ is defined as the composition of a spatial relation with an object. Notice that the space of regions is defined by the uniquely defined objects in the environment model. The spaces of spatial relation and object classes are also applied for behavior inference. The space of modes $\Gamma^{\mathcal{M}}$ defines variations of actions that influence the cost functions used to determine the optimal plan. Mode types such as "safe" and "quickly" given the same set of goals may, for example, produce different actions in the same environment. Lastly, the space of actions $\Gamma^{\mathcal{A}_\mathcal{O}}$ is defined by a unique object, spatial relation, reference object, and action type $\mathcal{A}_\mathcal{O}$. The space of spatial relation classes is additionally used in behavior inference. The space of symbols for behavior inference $\Gamma^{\mathcal{B}}$ is defined by an object, spatial relation class, region, and action symbols.

$$\Gamma^B = \left\{\Gamma^{\mathcal{O}} \cup \Gamma^{\mathcal{S}} \cup \Gamma^{\mathcal{O}_\mathcal{C}} \cup \Gamma^{\mathcal{R}_\mathcal{O}} \cup \Gamma^{\mathcal{M}} \cup \Gamma^{\mathcal{A}_\mathcal{O}}\right\}, \tag{5a}$$

where the new constituent symbol spaces are defined as

$$\Gamma^{\mathcal{M}} = \{m_i | m_i \in \mathcal{M}\} \tag{5b}$$
$$\Gamma^{\mathcal{O}} = \{\gamma_{o_i} | o_i \in \mathcal{O}\} \tag{5c}$$
$$\Gamma^{\mathcal{R}_\mathcal{O}} = \left\{\gamma_{o_j}^{s_i} | s_i \in \mathcal{S}, o_j \in \mathcal{O}\right\} \tag{5d}$$
$$\Gamma^{\mathcal{A}_\mathcal{O}} = \left\{\gamma_{o_j,o_k}^{s_i,a_{o_m},m_n} | s_i \in \mathcal{S}, o_j \in \mathcal{O}, o_k \in \mathcal{O}, a_{o_m} \in \mathcal{A}_\mathcal{O}, m_n \in \mathcal{M}, \right\} \tag{5e}$$
$$\tag{5f}$$

These symbols generally describe a uniform representation of the search space for the experiments described in Section 4. Note that the complexity of these symbolic representations can be increased or decreased depending on the diversity of tasks explored in the application of this framework. Existing works (Paul et al., 2016, 2018) consider grounding natural-language expressions in relation to inferred object sets, however this is not studied here.

3.3 Semantic Mapping

Integral to our approach is the ability to exploit environment-related information implicit in the natural-language instruction to maintain a distribution over the world model. Here, we detail a Bayesian filtering-based approach to maintaining this distribution. We represent the world model as a modified *semantic graph* (Walter et al., 2013) $S_t = \{G_t, X_t, L_t\}$, a hybrid metric, topological, and semantic representation of the robot's environment, which we visualize in Figure 5.

The topology G_t consists of a set of nodes that represent objects (e.g., boxes, balls, cones, etc.) and places (e.g., offices, lobbies, etc.) in the environment that have either been observed or visited by the robot, or are hypothesized based upon language. Nodes are partitioned into regions $R_i = \{n_1, n_2, \ldots, n_m\}$ that represent spatially coherent areas (e.g., rooms and hallways), which we refer to as *spatial regions*, as well as individual objects (e.g., boxes), which we refer to as *object regions*. Object regions typically consist of a single node. Edges in the topology model spatial relationships between nodes, and reflect the robot's motion, or constraints inferred from language. More specifically, similar to pose graph formulations of SLAM (Eustice et al., 2005; Olson et al., 2006; Kaess et al., 2008), an edge connects two nodes (locations) that the robot has transitioned between or nodes (objects or places) that it has observed, as well as nodes for which language indicates the existence of a specific spatial relation (e.g., that the kitchen is "down" the hallway or that there is a ball "inside" a box). We associate a pose x_i with each node n_i. The concatenation of these poses constitutes the metric map X_t. The semantic layer L_t expresses the semantic attributes of each spatial and object region, which include its colloquial name and type l_{R_i}.

Annotations that are inferred from a given instruction under our language model provide information regarding the existence, type, and location (relative to the robot or another landmark) of entities in the environment. We learn a distribution over possible world models consistent with these annotations by treating them as observations α_t in a filtering framework, effectively treating language as another sensing modality. We combine these observations with those from other sensors onboard the robot (e.g., LIDAR

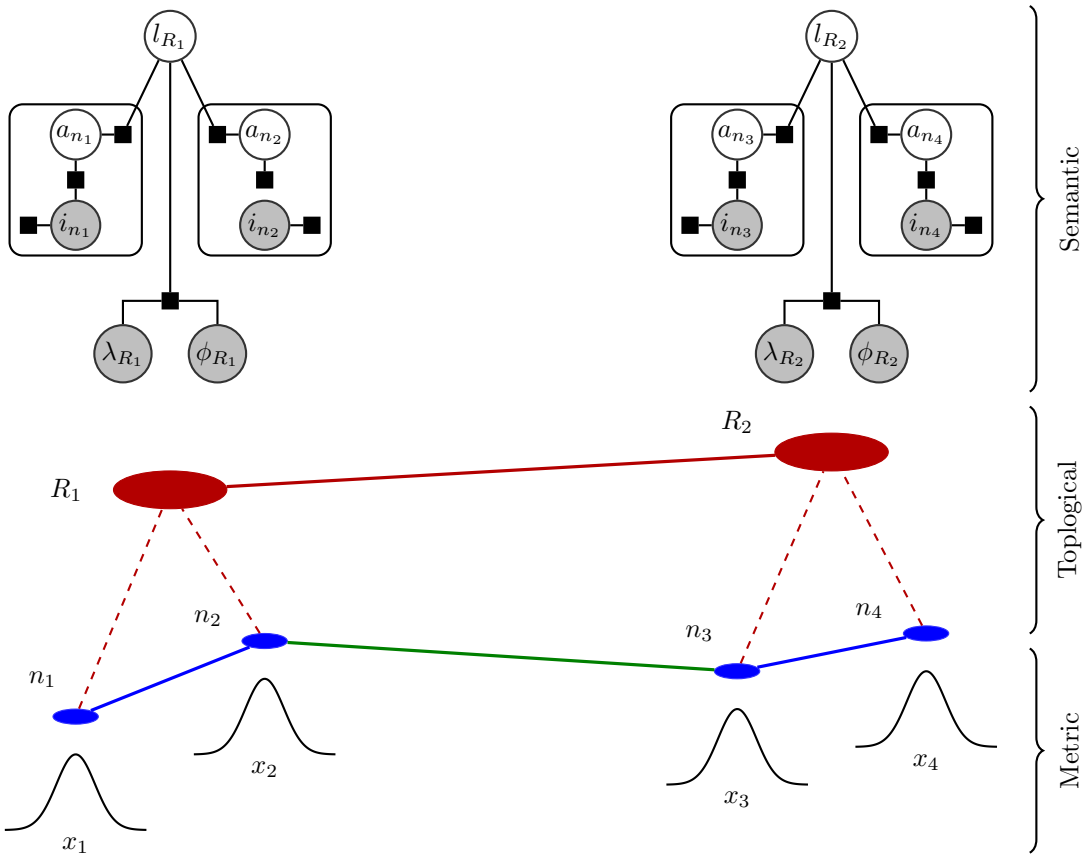

Figure 5: The semantic graph S_t models the metric (spatial), topological, and semantic properties of the environment. The topology G_t consists of a set of nodes that represent objects and locations in the environment that have either been observed or visited by the robot, or are hypothesized based upon language. Each node is associated with a region R_i that represents spatially coherent areas in the environment. Edges in the topology, where intra- and inter-region edges are rendered in blue and green, respectively, and model spatial relationships between nodes, reflect the robot's motion, observations, or constraints inferred from language. The edge rendered in red between the two regions is for visualization purposes only. The topology induces a pose graph, which corresponds to the metric map X_t. The semantic layer L_t models the category l_{R_j} of each region R_j, which we infer from language λ_{R_j} and node-level scene and object classifiers i_{n_k}.

and camera-based object and spatial region appearance observations) z_t to maintain a distribution over the semantic map:

$$p(S_t|\Lambda^t, z^t, u^t) \approx p(S_t|\alpha^t, z^t, u^t) \tag{6a}$$

$$= p(G_t, X_t, L_t|\alpha^t, z^t, u^t) \tag{6b}$$

$$= p(L_t|X_t, G_t, \alpha^t, z^t, u^t)\, p(X_t|G_t, \alpha^t, z^t, u^t)\, p(G_t|\alpha^t, z^t, u^t), \tag{6c}$$

where we replace the utterance Λ^t with the set of inferred annotations α_t (Sec. 3.2). The factorization in the last line models the metric map as being induced by the topology, much like is done with pose graph approaches to SLAM (Kaess et al., 2008).

In theory, the set of possible graphs for any given environment is combinatorial, because the number of edges can be exponential in the number of nodes. This suggests that it would be intractable to maintain a full distribution over the set of graphs for all but trivially small environments. To simplify this complexity, we adopt an assumption made by others (Ranganathan and Dellaert, 2011)) that the distribution is dominated by only a few topologies. More specifically, unless the environment is perceptually aliased, a large number of particles will be inconsistent with the robot's observations and will thus be assigned low likelihood.

Conditioning on the environment annotations further supports this assumption as it decreases the probability of edges that are inconsistent with the command. Any structure in the environment will also bound the interconnectivity of nodes (e.g., walls occluding the robot's LIDAR prevent observations of an adjacent room that would otherwise result in an edge to the node that denotes the robot's pose) as does the limited field-of-view of the robot's sensors, further increasing the number of topologies having near-zero likelihood. Consequently, only a few topologies that are consistent with the observations and annotations will be associated with non-negligible likelihoods. In environments for which this assumption does not hold (e.g., open areas with objects distributed sparsely throughout), our framework can still be used, but the computational cost will increase due to the need to maintain a distribution over the larger set of topologies.

Leveraging this assumption, we use a sample-based representation of the posterior distribution over graphs $p(G_t|\alpha^t, z^t, u^t)$ in Equation 6c. Specifically, we maintain the factored semantic map distribution using a Rao-Blackwellized particle filter (RBPF) (Doucet et al., 2000), where we employ a sample-based representation of the distribution over the environment topology $p(G_t|\alpha^t, z^t, u^t)$ and a Gaussian representation of the metric (pose) distribution $p(X_t|G_t, \alpha^t, z^t, u^t)$ that is induced by the topology. We parameterize the Gaussian pose distribution in the canonical (information) form, i.e., in terms of the information (inverse covariance) matrix and information vector, as opposed to the standard covariance form. The structure of the information matrix follows that of the topology (Eustice et al., 2005; Walter et al., 2007; Kaess et al., 2008), which is sparse for typical environments, thereby allowing us to exploit this sparsity to improve the efficiency of inference (Thrun et al., 2004; Eustice et al., 2005; Kaess et al., 2008; Walter et al., 2007).

We model the semantic distribution $p(L_t|X_t, G_t, \alpha^t, z^t, u^t)$ using a factor graph, which we visualize in plate notation in Figure 5 (top). The factor graph includes a random variable for each region that expresses its type (i.e., category) l_{R_i}. The factor graph includes variables that express language-based annotations, where the node λ_{R_i} denotes a potential reference to region R_i in the natural-language utterance, while ϕ_i is a Boolean variable that specifies whether or not the reference corresponds to the region. For each node n in the region, the robot makes indirect observations of the region's appearance a_n, which is coupled with the region's category, via image-based scene classifiers i_n.

Together, this gives rise to the following parameterization of the posterior

$$\mathcal{P}_t = \left\{ P_t^{(1)}, P_t^{(2)}, \ldots, P_t^{(n)} \right\}, \tag{7}$$

where each particle $P_t^{(i)}$ includes a candidate topology $G_t^{(i)}$, Gaussian pose graph $X_t^{(i)}$, semantic map $L_t^{(i)}$, and particle weight $w_t^{(i)}$

$$P_t^{(i)} = \left\{ G_t^{(i)}, X_t^{(i)}, L_t^{(i)}, w_t^{(i)} \right\} \tag{8}$$

The robot detects and labels objects in the environment based on camera observations, using a neural object detector built on top of the YOLO V3 architecture (Redmon and Farhadi, 2018). A neural image-based scene classifier also provides noisy observations of the semantic class of spatial regions. In addition to assigning labels, we use the inferred scene classes to segment spatial regions, using the presence of conflicting appearance labels to suggest a region segmentation. As we describe next, we couple this with a spectral clustering-based measure of the spatial coherence between laser scans in order to refine the boundaries of spatial regions. Since this clustering reasons over the similarity of laser scans associated with different nodes, it typically segments a region after the robot last observes it. However, using inferred scene classes allows the method to be aware of new regions when they are first observed, enabling us to immediately evaluate each particle's likelihood based on the observation of region appearance. In turn, we can down-weight particles that are inconsistent with the actual layout of the world sooner, reducing the number of actions the robot must take to satisfy the command.

We maintain each particle through the three steps of the RPBF as detailed in Algorithm 1. First, we propagate the topology by sampling modifications to the graph when the robot receives new sensor observations or annotations. Second, we perform a Bayesian update to the pose distribution based upon the sampled modifications to the underlying graph. Third, we update the weight of each particle based on the likelihood of generating the given observations, and resample as needed to avoid particle depletion. We now outline this process in more detail.

Algorithm 1: Semantic Mapping Algorithm

Input: $P_{t-1} = \left\{P_{t-1}^{(i)}\right\}$, and $(u_t, z_t, a_t, \alpha_t)$, where $P_{t-1}^{(i)} = \left\{G_{t-1}^{(i)}, X_{t-1}^{(i)}, L_{t-1}^{(i)}, w_{t-1}^{(i)}\right\}$

Output: $P_t = \left\{P_t^{(i)}\right\}$

for $i = 1$ *to* n **do**

1. Employ proposal distribution $p(G_t|G_{t-1}^{(i)}, z^{t-1}, u^t, \alpha^t)$ to propagate the graph sample according to odometry on u_t, the inferred region labels l_t, and scene classifications z_t.
   (a) Sample region allocation
   (b) Sample region edges
   (c) Merge newly connected regions
2. Update the Gaussian distribution over the node poses $X_t^{(i)}$ according to the constraints induced by the newly-added graph edges.
3. Update the factor graph representing semantic properties for the topology based on appearance observations z_t and language-based annotations α_t.
4. Compute the new particle weight $w_t^{(i)}$ based upon the previous weight $w_{t-1}^{(i)}$ and the metric data z_t.

end

Normalize weights and resample if needed, i.e., if $N_{\text{eff}} < n/2$, where $N_{\text{eff}} = \frac{1}{\sum_{i=0}^{n} w_i^2}$.

3.3.1 The Proposal Distribution

We compute the predictive posterior over the graph G_t using a proposal that is the distribution over the current graph given the previous graph G_{t-1}, sensor data (excluding the current time step), appearance data, odometry, and language

$$p(G_t|G_{t-1}^{(i)}, z^{t-1}, u^t, \alpha^t). \tag{9}$$

For each particle $P_{t-1}^{(i)}$, we update the topology $G_{t-1}^{(i)}$ according to the robot's motion, annotations inferred from language, and environment observations. In particular, we first add a node n_t that denotes the robot's current pose and an edge between it and the previous node that encodes the temporal (odometry) constraint between the two poses.[2] We initially assign the new node to the nearest region, which most often is that of the previous node, resulting in an intermediate graph $G_t^{(i)-}$.[3] We then propose modifications to the graph $\Delta_t^{(i)} = \{\Delta_{t,\alpha}^{(i)}, \Delta_{t,z}^{(i)}\}$ based upon appearance observations $\Delta_{t,z}^{(i)}$ and natural-language annotations $\Delta_{t,\alpha}^{(i)}$:

$$p(G_t^{(i)}|G_{t-1}^{(i)}, z^{t-1}, u^t, \alpha^t) = p(\Delta_{t,\alpha}^{(i)}|G_t^{(i)-}, \alpha^t)\, p(\Delta_{t,z}^{(i)}|G_t^{(i)-}, z^{t-1})\, p(G^{(i)-}|G_{t-1}^{(i)}, u_t), \tag{10}$$

where we define the three distributions on the right-hand side below. This formulation updates the graph $G_t^{(i)-}$ with modifications $\Delta_t^{(i)}$ that can include the addition and deletion of nodes and regions, as well as the addition of edges that model spatial relations inferred from environment observations and natural language-based annotations. We sample graph modifications from two independent proposal distributions, one for those that reflect annotations α_t and the other that reflects traditional observations z_{t-1}.

Updating the current spatial region The term $p(G^{(i)-}|G_{t-1}^{(i)}, u_t)$ in Equation 10 is the distribution that follows from adding the node and edge that account for the robot's motion. which results in the intermediate graph $G_t^{(i)-}$. We then probabilistically bisect the robot's current spatial region R_c using the

[2] We add a node corresponding to the robot's current pose when it observes a new object or spatial region, or has traveled more than a specified distance. In practice, we typically use 1.0 m as the distance threshold.

[3] This and the remainder of this discussion apply to individual particles, however we remove the particle label for readability.

spectral clustering method proposed by Blanco et al. (2006). We generate the similarity matrix based on the overlap between the laser scans associated with each pair of nodes in the spatial region. Equation 11 defines the likelihood of bisecting the region, which is based on the normalized cut value N_c of the graph involving the proposed segments. The likelihood of accepting a proposed segmentation increases as the value of N_c decreases, i.e., as the separation of the two segments increases (minimizing the inter-region similarity).

$$P(s/N_{cut}) = \frac{1}{(1 + \alpha N_c^3)} \tag{11}$$

The result is that areas that are more spatially distinct have a greater probability of being represented as separate spatial regions, i.e., more particles will model these regions as distinct. If a particle chooses to segment the current region, it creates a new spatial region R_i that does not include the newly added node.

Modifying the graph based on observations In the event that the algorithm creates a new region R_i via segmentation, it then considers connecting the new region to existing regions in the topology, including those that are hypothesized based on language. The method samples edges to observed regions using a spatial distribution that is a function of the regions' constituent nodes. We refer to these modifications to each particle as $\Delta_{t,z}^{(i)}$, giving rise to the corresponding distribution from Equation 10

$$p(\Delta_{t,z}^{(i)} | G_t^{(i)-}, z^{t-1}, u^t, \alpha^{t-1}) = \prod_{j: e_{ij} \notin E_t^-} p(G_t^{ij} | G_t^{(i)-}, z^{t-1}, u^t, \alpha^{t-1}) \tag{12}$$

Here, we assume that additional edges expressing constraints that involve the current node $e_{ij} \notin E_t^-$ are conditionally independent.

We model the spatial distribution prior in terms of the distance d_{ij} between the nodes in each of the two regions that are nearest to the center of the region

$$p(G_t^{ij} | G_t^{(i)-}, z^{t-1}, u^t, \alpha^{t-1}) = \int_{X_t^-} p(G_t^{ij} | X_t^-, G_t^{(i)-}, z^{t-1}, u^t, \alpha^{t-1}) \, p(X_t^- | G_t^{(i)-}, z^{t-1}, u^t, \alpha^{t-1}) \tag{13a}$$

$$\approx \int_{d_{ij}} p(G_t^{ij} | d_{ij}, G_t^{(i)-}, z^{t-1}, u^t, \alpha^{t-1}) \, p(d_{ij} | G_t^{(i)-}, z^{t-1}, u^t, \alpha^{t-1}). \tag{13b}$$

The conditional distribution $p(G_t^{ij} | d_{ij}, G_t^{(i)-}, z^{t-1}, u^t, \alpha^{t-1})$ expresses the likelihood of adding an edge between spatial regions R_i and R_j based upon the location of their mean nodes. We represent the distribution for a particular edge between regions R_i and R_j with distance $d_{ij} = |\bar{X}_{R_i} - \bar{X}_{R_j}|_2$ as

$$p(G_t^{ij} | d_{ij}, G_t^{(i)-}, z^{t-1}, u^t, \alpha^{t-1}) = p(G_t^{ij} | d_{ij}) \propto \frac{1}{1 + \gamma d_{ij}^2}, \tag{14}$$

where γ expresses a distance bias.[4] We approximate the distance prior $p(d_{ij} | G_t^{(i)-}, z^{t-1}, u^t, \alpha^{t-1})$ with a folded Gaussian distribution.

Merging with observed or hypothesized regions After adding a new spatial region R_i and any inter-region edges, we then evaluate whether to merge the region with any of the regions to which it is connected. We merge the region with an existing (connected) region if the modes of their distributions over region type (i.e., category) are the same. This results in regions being merged when the robot revisits locations already represented in the graph. This merge process is designed such that the complexity of the topology increases only when the robot explores new areas, leading to more efficient region edge proposals as well as more compact language groundings.

If the newly added spatial region was not merged with one that was previously visited, or when an object region was added based upon camera observations, we check whether it matches a region that was previously hypothesized based on an annotation (for example, a toolbox that the robot detected may be the same one that was hypothesized earlier based on the instruction). We do so by sampling a grounding

[4] In practice, we have found $\gamma = 0.3$ to work well empirically.

to any unobserved regions in the topology using a Dirichlet process prior. If this results in a grounding to an existing hypothesized region, we remove the hypothesized region and adjust the topology accordingly, resampling any edges to yet-unobserved regions. For example, if an annotation suggested the existence of a "toolbox inside the garage," and we grounded the robot's current region to the hypothesized garage, we would reevaluate the "inside" relation for the hypothesized toolbox with respect to this detected garage.

Modifying the graph based on natural language In the third part of the proposal step (Eqn. 10), we sample modifications to the graph for each particle based on (the possibly empty) set of annotations $\alpha_t = \{\alpha_{t,j}\}$ using a factored form of the distribution:

$$p(\Delta^{(i)}_{t,\alpha}|S^{(i)-}_t, \alpha_t) = \prod_j p(\Delta^{(i)}_{\alpha_{t,j}}|S^{(i)-}_t, \alpha_{t,j}). \tag{15}$$

An annotation $\alpha_{t,j}$ contains a spatial relation and figure when the language describes one region (e.g., "go to the elevator lobby"), and an additional landmark when the language describes the relation between two regions (e.g., "retrieve the wrench from inside the toolbox" or "get the mug from the kitchen"), which may be spatial or object regions. We use a likelihood model over the spatial relation to sample landmark and figure pairs for the grounding. This model employs a Dirichlet process prior that accounts for the fact that the annotation may refer to regions that exist in the map or to regions that are currently unknown. For each landmark and/or region that is sampled as being new, we add a new node to the graph and assign the node to its own region. We then add an edge between the figure and landmark and define the metric constraint associated with this edge based on the spatial relation. We represent the distribution associated with this constraint as a Gaussian with a mean expressed as a linear function of features that describe the locations of the regions, their bounding boxes, and the robot's location at the time of the utterance. We learn this function along with the covariance of the Gaussian using a natural-language corpus of spatial relations (Tellex et al., 2011).

3.3.2 Updating the metric map based on new edges

The proposal step results in an update to the graph $G^{(i)}_t$ associated with each particle that includes the addition of a node representing the robot's current pose, the addition of edges, and the possible creation and merging of regions. These modifications need to then be reflected in the distribution over poses. To that end, we first augment the pose vector X^-_t to include the robot's current pose. We then incorporate the relative pose constraints expressed by the new edges, including the temporal (odometry) edge between the current and previous poses, into the Gaussian representation for the marginal distribution over the pose history

$$p(X_t|G_t, \alpha^t, z^t, u^t) = \mathcal{N}^{-1}(X_t; \Sigma^{-1}_t, \eta_t), \tag{16}$$

where Σ^{-1}_t is the information (inverse covariance) matrix and η_t is the information vector that together parameterize the canonical form of the Gaussian.[5] Key to this parameterization is that it corresponds to a Gaussian Markov random field, whereby the structure of the information matrix is given by the topology of the underlying graph. Specifically, the off-diagonal blocks of the information matrix relating pose x_i and pose x_j are non-zero if and only if there is an edge in the graph between the corresponding nodes n_i and n_j. For any new edge added to the graph during the proposal step, we update the corresponding entries of the information matrix following the standard information filtering procedure (Eustice et al., 2005; Walter et al., 2007; Kaess et al., 2008). We refer the reader to Walter et al. (2007) for a description of this process. Critically, the sparsity of the information matrix is determined by the underlying graph G_t, which is generally sparse for typical environments. We exploit this sparsity to improve the computational cost of inference (Paskin, 2003; Thrun et al., 2004; Eustice et al., 2005; Walter et al., 2007; Kaess et al., 2008). In particular, we utilize the iSAM algorithm (Kaess et al., 2008) to update the canonical form by iteratively solving for the QR factorization of the information matrix. We refer the reader Kaess et al. (2008) for the details of this process.

[5] We maintain separate parameters for each particle, but omit the superscript indicating the particle ID for readability.

3.3.3 Re-weighting particles and resampling

After modifying each particle's topology, we perform a Bayesian update to its Gaussian distribution. We then re-weight each particle according to the likelihood of generating language annotations and region appearance observations:

$$w_t^{(i)} = p(z_t, \alpha_t | S_{t-1}^{(i)}) w_{t-1}^{(i)} = p(\alpha_t | S_{t-1}^{(i)}) p(z_t | S_{t-1}^{(i)}) w_{t-1}^{(i)}. \tag{17}$$

When calculating the likelihood of each region appearance observation, we consider the current node's region type and calculate the likelihood of generating this observation given the topology. In effect, this down-weights any particle with a sampled region of a particular type existing on top of a known traversed region of a different type. We use a likelihood model that describes the observation of a region's type, with a latent binary variable v that denotes whether or not the observation is valid. We marginalize over v to arrive at the likelihood of generating the given observation, where R_u is the set of unobserved regions in particle $S_{t-1}^{(i)}$:

$$p(z^t | S_{t-1}^{(i)}) = \prod_{R_i \in R_u} \left(\sum_{v \in 1,0} p(z^t | v, R_i)\ p(v | R_i) \right). \tag{18}$$

We define the probability of annotations $p(\alpha_t | S_{t-1}^{(i)})$ as the language grounding likelihood under the map at the previous time step (Sec. 3.2). As such, a particle with an existing pair of regions that conform to a specified language constraint will be weighted higher than one without. In an effort to avoid particle depletion, we resample the particles when the variance of the weights exceeds a threshold, as measured by the number of effective particles (Doucet, 1998)

$$N_{\text{eff}} = \frac{1}{\sum_{i=0}^{n} w_i^2}. \tag{19}$$

In the experiments conducted in this paper, we set the threshold to half of the number of particles.

3.4 Planning Under Uncertainty

It is intractable to search over the complete trajectory that is optimal in the distribution over maps. Instead, we formulate instruction-following in unknown environments as a planning under uncertainty problem, whereby we seek a policy π that minimizes the one-step expected cost c.

In earlier work (Duvallet et al., 2013), the cost was a function of a single topological representation of the environment, which included nodes that were previously visited as well as those that represent frontiers in the environment. In this work, however, the planner must reason over a *distribution* over semantic maps as opposed to a single world model. Thus, we express the cost c as a function of the robot's current pose x_t, the available actions $a_t \in A_t$, and the map distribution $p(S_t)$

$$\pi\left(x_t, p(S_t)\right) = \arg\min_{a \in A_t} c\left(x_t, a_t, p(S_t)\right), \tag{20}$$

where the belief-space actions include paths from the robot's current pose to each node (landmark) in the graph $v_t \in G_t$, paired with the distribution over the nodes. The action space also includes an explicit stop action a_{stop} that declares that the planner has satisfied the instruction.

$$A_t = \{\text{path}(x_t, v_t) \times p(v_t)\ \forall v_t \in G_t\} \cup \{a_{\text{stop}}\} \tag{21}$$

In this manner, the planner differentiates between landmarks that the robot has detected and thus have low uncertainty, and those that are hypothesized from language and correspondingly more uncertain. Represented in this way, the robot can choose to explore unknown locations (e.g., continuing to search the hallway or navigating to a box that is hypothesized as containing the ball), backtrack when a previous action hasn't been fruitful (e.g., traveling to the wrong room or to an empty box), and stop when the planner concludes that the instruction has been satisfied.

The following sections explain how the policy reasons in belief space, and the novel imitation learning formulation to train the policy from demonstrations of correct behavior.

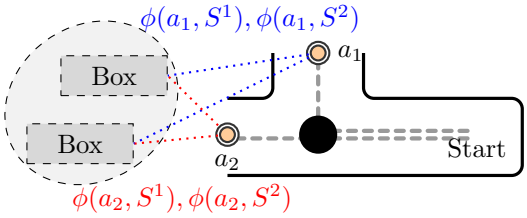

Figure 6: A simplified illustration of the computation of feature moments in the space of hypothesized landmarks. In this example, there are two hypothesized boxes. In order to determine the features over a landmark distribution, we compute the features for each action across all hypothesized landmark samples and aggregate by means of moment statistics.

3.4.1 Belief-Space Reasoning using Distribution Embedding

A standard choice for the cost function is to represent it as a linear combination of features over the current state and actions (Ratliff et al., 2006; Abbeel and Ng, 2004; Syed et al., 2008), where the state nominally includes the robot's pose, the semantic map, and the current time. However, rather than a single world model, the semantic map distribution $p(S_t)$ provides a distribution over the observed and hypothesized location of landmarks (i.e., objects and regions) relevant to the given natural-language instruction. As such, the policy π must represent and compute distances between *distributions* over action features when computing the cost of any action a_t.

Hilbert Space embeddings (Smola et al., 2007; Gretton et al., 2007) provide a convenient representation of distributions with which one can efficiently measure the distance between distributions via a pseudometric. We embed the distribution over action features in a Reproducing Kernel Hilbert Space (RKHS), using the mean feature map (Smola et al., 2007; Gretton et al., 2007) that consists of the first K moments of the features computed with respect to each map sample $S_t^{(i)}$ and its likelihood as a sample-based representation of the distribution

$$\hat{\Phi}_1(x_t, a_t, S_t) = \sum_{S_t^{(i)}} p(S_t^{(i)})\, \phi\left(x_t, a_t, S_t^{(i)}\right) \tag{22a}$$

$$\hat{\Phi}_2(x_t, a_t, S_t) = \sum_{S_t^{(i)}} p(S_t^{(i)})\, \left(\phi\left(x_t, a_t, S_t^{(i)}\right) - \hat{\Phi}_1\right)^2 \tag{22b}$$

$$\vdots$$

$$\hat{\Phi}_K(x_t, a_t, S_t) = \sum_{S_t^{(i)}} p(S_t^{(i)})\, \left(\phi\left(x_t, a_t, S_t^{(i)}\right) - \hat{\Phi}_1\right)^K. \tag{22c}$$

The vector $\phi(x_t, a_t, S_t^{(i)})$ is a concatenation of features that are a function of action a_t and a *single* landmark in $S_t^{(i)}$. These include geometric features that express the shape of the path associated with the action, such as the cumulative change in angle, which may be correlated with actions that go straight or that turn. They also include features that express the geometry of the landmark, such as the area of the landmark region, and relationships between the action and landmark, such as the difference between the distance from the landmark at the start and the distance at the end of the path, which may be correlated with going towards vs. away from the landmark. Please see our earlier work Duvallet et al. (2013) for a thorough description of these features.

This RKHS-based representation of the features (Eqn. 22) computes features individually for the action and all hypothesized landmarks in the sample-based representation of the map distribution. We aggregate these feature vectors, and then compute moments of the feature vector distribution (i.e., the mean, variance, and higher order statistics). Figure 6 provides a simple illustration of how we compute belief-space features for two actions with a hypothesized box that has two possible locations.

We express the cost function in Equation 20 as a weighted sum of the first K moments of the feature distribution (Eqn. 22):

$$c\left(x_t, a_t, S_t\right) = \sum_{k=1}^{K} w_k^\top \ \hat{\Phi}_k\left(x_t, a_t, S_t\right). \tag{23}$$

where w_k is the weight vector associated with moment k. Concatenating the weights and moments into column vectors $W = \begin{bmatrix} w_1 & \cdots & w_K \end{bmatrix}^\top$ and $F = \begin{bmatrix} \hat{\Phi}_1 & \cdots & \hat{\Phi}_K \end{bmatrix}^\top$, we can express the policy in Equation 20 as minimizing a weighted sum of the feature moments F_{a_t} for action a_t :

$$\pi\left(x_t, S_t\right) = \arg\min_{a_t \in A_t} W^\top F_{a_t}. \tag{24}$$

3.4.2 Imitation Learning Formulation

We train the policy using imitation learning whereby we treat the problem of predicting the action as a multi-class classification problem. Specifically, given an expert demonstration, we seek a policy that correctly predicts their chosen action among all possible actions for the same state. Our earlier work proposed the use of imitation learning for training a direction-following policy, however it assumes that the environment is at least partially known a priori (Duvallet et al., 2013). We make no such assumption here, and instead train a belief-space policy that reasons in a *distribution* of hypothesized maps, thereby supporting instances in which the agent has no a priori knowledge of the environment.

We assume that the expert's policy π^* minimizes the unknown immediate cost $c(x_t, a_t^*, S_t)$ of performing the demonstrated action a_t^* from state x_t, under the map distribution $p(S_t)$. However, since we cannot directly observe the true costs of the expert's policy, we must instead minimize a surrogate loss that penalizes disagreements between the expert's action a_t^* and the action a_t selected by the policy using the multi-class hinge loss (Crammer and Singer, 2002), computed over all demonstrations:

$$\ell\left(x_t, a_t^*, c, S_t\right) = \max\left(0, 1 + c\left(x_t, a_t^*, S_t\right) - \min_{a_t \neq a_t^*}\left[c\left(x_t, a_t, S_t\right)\right]\right). \tag{25}$$

Formulated in this manner, the policy selects an action that differs from that of the expert (i.e., $a_t \neq a_t^*$) if and only if the cost associated with that action ($c(x_t, a_t, S_t)$) is less than the cost of the expert's action ($c\left(x_t, a_t^*, S_t\right)$) by a margin of one. The loss can be re-written and combined with Equation 24 to yield:

$$\ell\left(x_t, a_t^*, W, S_t\right) = W^\top F_{a_t^*} - \min_{a_t}\left[W^\top F_{a_t} - l_{xa}\right], \tag{26}$$

where the margin $l_{xa} = 0$ if $a_t = a_t^*$ and $l_{xa} = 1$ otherwise. This ensures that the expert's action is better than all other actions by a margin (Ratliff et al., 2006). We further add a regularization term λ to Equation 26, yielding the complete optimization loss:

$$\ell\left(x_t, a_t^*, W, S_t\right) = \frac{\lambda}{2}\|W\|^2 + W^\top F_{a_t^*} - \min_{a_t}\left[W^\top F_{a_t} - l_{xa}\right]. \tag{27}$$

Although this loss function is convex, it is not differentiable. However, we can optimize it efficiently by taking the subgradient of Equation 27 and computing action predictions for the loss-augmented policy (Ratliff et al., 2006):

$$\frac{\partial \ell}{\partial W} = \lambda W + F_{a_t^*} - F_{a_t'} \tag{28}$$

where a_t' is the best loss-augmented action associated with state x_t (i.e., the solution to our policy using the loss-augmented cost):

$$a_t' = \arg\min_{a_t}\ \left[W^\top F_{a_t} - l_{xa}\right]. \tag{29}$$

The subgradient leads to the update rule for the weights W_t:

$$W_{t+1} \leftarrow W_t - \alpha\, \frac{\partial \ell}{\partial W} \tag{30}$$

with a learning rate $\alpha \propto 1/t^{\gamma}$. Intuitively, if the current policy disagrees with the expert's demonstration, Equation 30 decreases the weight (and thus the cost) for the features of the demonstrated action $F_{a_t^*}$, and increases the weight for the features of the planned action $F_{a_t'}$. If the policy produces actions that are consistent with the expert's demonstration, only the regularization term is updated. As in our prior work, we train the policy using the DAGGER algorithm (Ross et al., 2011), which learns a policy by iterating between collecting data (using the current policy) and applying expert corrections on all states visited by the policy (using the expert's demonstrated policy).

Treating direction following in the space of possible semantic maps as a problem of sequential decision making under uncertainty provides an efficient approximate solution to the belief-space planning problem. By using a kernel embedding of the distribution of features for a given action, our approach can learn a policy that reasons about the distribution of semantic maps.

4 Experiments

To evaluate the effectiveness of the proposed approach to natural-language instruction-following in a priori unknown environments, we performed experiments on the three different robotic systems illustrated in Figure 7. For each of these, we used a form of a symbolic representation for annotation inference and behavior inference that involved several different types of symbols.

(a) Clearpath Robotics Husky A200 UGV (b) Robotic Wheelchair (c) Clearpath Robotics Husky A200 UGV with a Universal Robotics UR5 Manipulator

Figure 7: The three robots used in physical experiments. The Clearpath Robotics Husky A200 UGV in (a) and the Robotic Wheelchair in (b) were used for experiments involving following of route instructions in Section 5.1.2 while the Clearpath Robotics Husky A200 UGV outfitted with a Universal Robotics UR5 manipulator in (c) was used for natural language understanding for mobile manipulation in Section 5.2

The first system evaluated was an unmanned ground vehicle. For annotation and behavior inference for these experiments we assumed seven different spatial relation types $\mathcal{S}$ ("unknown", "near", "away", "front", "back", "left", "right"), eight object types $\mathcal{O}_{\mathcal{C}}$ (" unknown", "robot", "cone", "tree", "car", "building", "hydrant", and "wall") and no location types. For the space of behaviors, we considered two possible action types $\mathcal{A}_{\mathcal{O}}$ ("unknown" and "navigation") and three possible modes $\mathcal{M}$ ("safely", "quickly", and "unknown"). For symbol grounding, both annotation and behavior inference used the DCG model Howard et al. (2014b) with a corpus of 39 fully labeled examples. Additional information on the symbolic representation and corpus used in the experiments can be found in Duvallet et al. (2014).

The second system evaluated was a robotic wheelchair. This system was evaluated in an office building environment. For both annotation and behavior inference, we assumed 12 different spatial relation types $\mathcal{S}$ ("unknown", "near", "away", "front", "back", "left", "right", "down", "through", "towards", "past", and "around") and 17 object and location types. Specifically, we used eight object types $\mathcal{O}_{\mathcal{C}}$ ("unkown",

"robot", "cone", "tree", "car", "building", "hydrant", and "wall") and nine location types $\mathcal{L}$ ("generic", "kitchen", "office", "hallway", "lab","lounge", "elevator", "conference room", and "cafeteria"). These experiments also included twelve spatial relation types. For the space of behaviors, we considered four possible actions ("unknown", "navigation", "right", and "left") and three possible modes $\mathcal{M}$ ("safely", "quickly", and "unknown"). For annotation inference and behavior inference, we used the HDCG Chung et al. (2015) model with a corpus of 54 fully labeled examples. More information about the symbolic representation used in these experiments can be found in Hemachandra et al. (2015).

The third system that we evaluated was a mobile manipulator consisting of a Clearpath Robotics Husky A200 Unmanned Ground Vehicle outfitted with a Universal Robotic UR5 manipulator and Robotiq Adaptive Robotic Gripper. We conducted experiments in both indoor and outdoor environments with a series of instructions that required the robot to both navigate and manipulate objects. A subset of these objects were selected from the YCB dataset Calli et al. (2015). For annotation inference, the object types $\mathcal{O}_\mathcal{C}$ included "drill", "suitcase", "banana", "pitcher", "cracker box", "mustard bottle", "ball", "box", and "cone", the location types $\mathcal{L}$ included "lab", "hallway", and "office", and the spatial relation types $\mathcal{S}$ included "inside", "behind", "left", "right", "front", and "back". For behavior inference, the action types $\mathcal{A}_\mathcal{O}$ included "pick", "retrieve", and "navigate", the object types $\mathcal{O}_\mathcal{C}$ included "drill", "suitcase", "banana", "pitcher", "cracker box", "mustard bottle", "ball", "box", and "cone", and the spatial relation types $\mathcal{S}$ included "inside" and "behind". No model types were used for the mobile manipulation experiments. For symbol grounding, both annotation and behavior inference used the DCG model Howard et al. (2014b) with a corpus of 115 fully labeled examples. The corpus contained instructions such as "Pick up the drill behind the cone", "Pick up the pitcher", "Go to the mustard bottle", "Retrieve the crackers box inside the box" etc. Additional information on the symbolic representation and corpus used in the experiments can be found in Patki et al. (2020).

5 Experimental Results

In the following, we discuss the results of the various experiments intended to evaluate the performance of our framework. We first consider the experiments focused on route instruction-following with the different robot platforms. We then analyze the results of the experiments that task a robot with carrying out natural language commands that involve mobile manipulation.

5.1 Instruction Following for Robot Navigation

We evaluated our algorithm's ability to follow route instructions in a priori unknown environments through experiments conducted in simulation as well as those involving the Husky and wheelchair robots. For comparison, we include a "Known Map" ground-truth baseline that performs language understanding with the environment being completely known. In this manner, the baseline provides an upper-bound on the performance of our framework.

5.1.1 Monte Carlo Simulations

Object-relative navigation We begin with a series of Monte Carlo simulation-based evaluations of our framework for the task of following natural language route directions. The first set of experiments considers a simple setup in which a Husky A200 Unmanned Ground Vehicle navigates an open environment consisting of different combinations of objects. We consider four environment templates, with different numbers of hydrants and cones. For each configuration, we sample ten environments, each with different object poses. For these environments, we issued three natural language instructions "go to the hydrant," "go to the hydrant behind the cone," and "go to the hydrant nearest to the cone." We note that these commands were not part of the corpus that we used to train the DCG model. Additionally, we considered six different settings for the robot's field-of-view, 2 m, 3 m, 5 m, 10 m, 15 m, and 20 m, and performed approximately 100 simulations for each combination of the environment, command, and field-of-view. As a ground-truth baseline, we performed ten runs of each configuration with a completely known world model.

Table 1 presents the success rate and distance traveled by the robot for these 100 simulation configurations. We considered a run to be successful if the planner stops within 1.5 m of the intended goal. Comparing

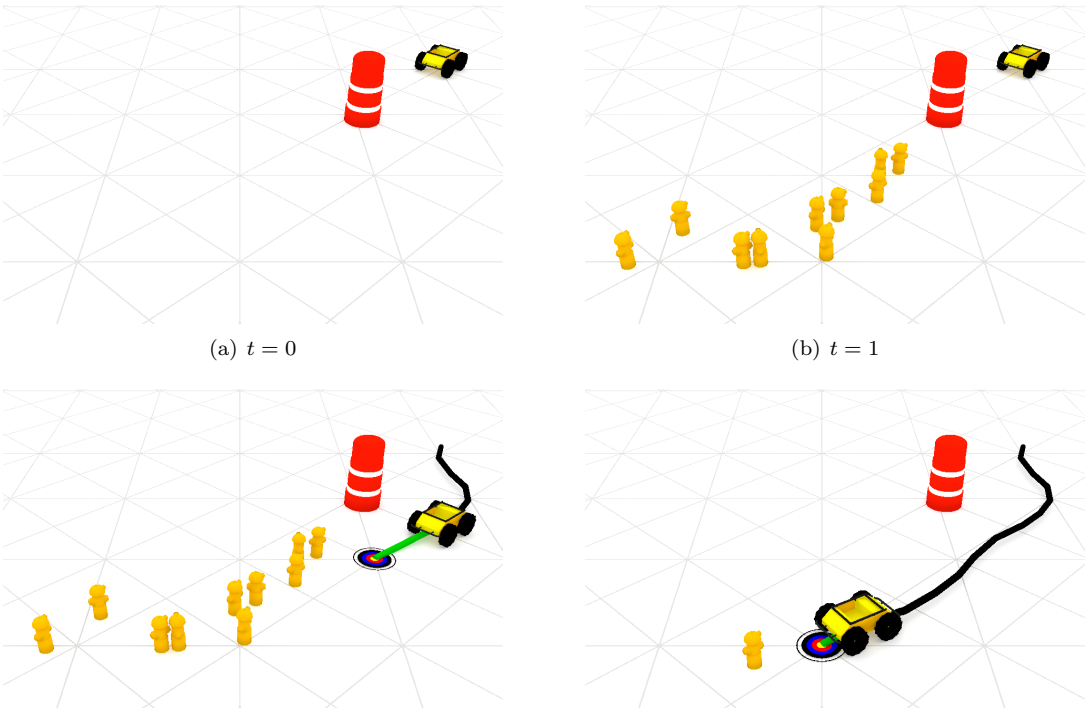

(a) $t = 0$ (b) $t = 1$

(c) $t = 2$ (d) $t = 3$

Figure 8: The evolution of our framework for a simulation-based experiment that tasks the Husky with following the instruction "go to the hydrant behind the cone". When the robot receives the command, (a) the traffic cone is visible, but not the hydrant, which is occluded by the cone. Our algorithm (b) proposes a distribution over the environment that effectively hypothesizes the location of the hydrant, which we visualize as the mean location for each of the particles. Based on this distribution, (c) the imitation learning-based policy decides to navigate behind the cone. At this point, (d) the robot observes the hydrant upon which the environment distribution effectively converges to the location of the detected hydrant (in practice, the distribution will still assign small, but non-zero likelihood for the hydrant being located elsewhere), which the policy then identifies as the goal.

Table 1: Monte Carlo simulation results with 1σ confidence intervals for the Husky experiments.

Environment		FOV (m)	Relation	Success Rate (%)		Distance (m)	
				Known	Ours	Known	Ours
1 hydrant	1 cone	3.0	null	100.0	93.9	8.75 (1.69)	16.78 (7.90)
1 hydrant	1 cone	3.0	"behind"	100.0	98.3	8.75 (1.69)	13.43 (7.02)
1 hydrant	2 cones	3.0	null	100.0	100.0	11.18 (1.38)	32.54 (18.50)
1 hydrant	2 cones	3.0	"behind"	100.0	99.5	11.18 (1.38)	40.02 (29.66)
2 hydrants	1 cone	3.0	null	100.0	54.4	10.49 (1.81)	21.56 (10.32)
2 hydrants	1 cone	3.0	"behind"	100.0	67.4	10.38 (1.86)	18.72 (10.23)
2 hydrants	1 cone	5.0	"nearest"	100.0	46.2	9.19 (1.54)	12.05 (5.76)

against commands such as "go to the hydrant" that do not provide an explicit spatial relation, the results demonstrate that our algorithm achieves greater success and yields more efficient paths by taking advantage of relations in the command (i.e., "go to the hydrant behind the cone"). This is apparent in environments that consist of a single hydrant as well as more ambiguous environments that consist of two hydrants. Particularly telling is the variation in performance as a result of different fields-of-view. Figure 9 shows how the success rate increases and the distance traveled decreases as the robot's sensing range increases, quickly

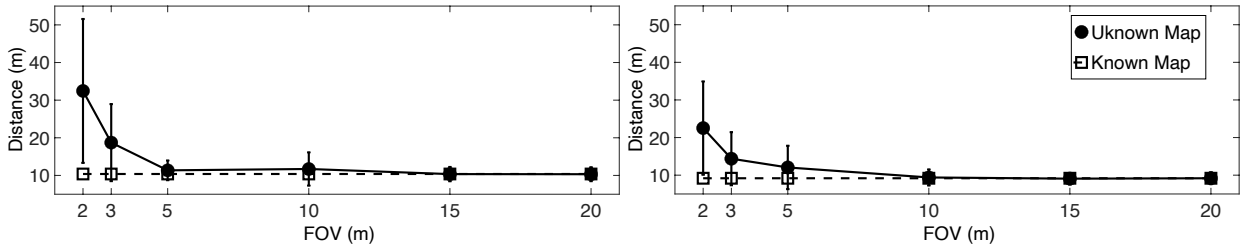

(a) Distance traveled for "behind" relation

(b) Distance traveled for "nearest" relation

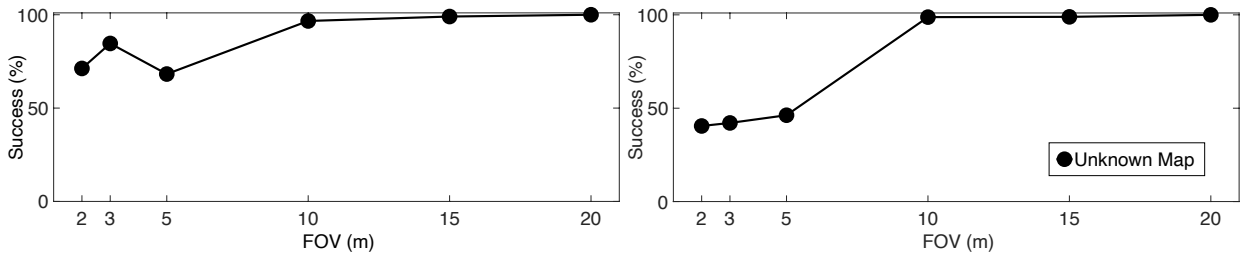

(c) Success rate for "behind" relation

(d) Success rate for "nearest" relation

Figure 9: Plots of the (top) distance traveled and (bottom) success rate as a function of the field-of-view for the commands (left) "go to the hydrant behind the cone" and (right) "go to the hydrant nearest to the cone" in simulation.

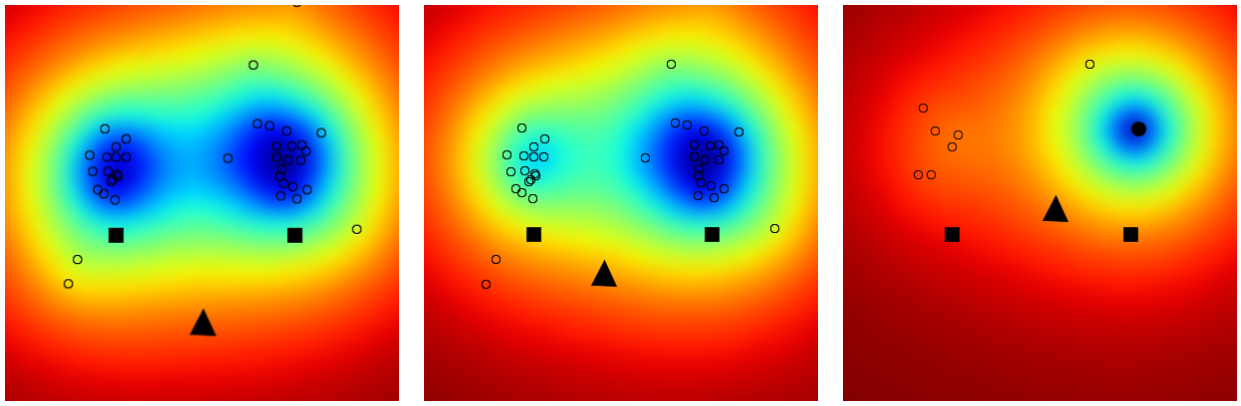

(a) $t = 0\,\text{sec}$

(b) $t = 4\,\text{sec}$

(c) $t = 8\,\text{sec}$

Figure 10: A visualization of the evolution of the semantic map distribution over time for the command "go to the hydrant behind the cone," where the triangle denotes the robot's location, squares represent observed cones, and circles denote hydrants that are either hypothesized (open) or observed (filled). (a) The robot starts off observing both cones, and hypothesizes possible hydrants that are consistent with the command. (b) The robot moves towards the left cluster, but having not observed the hydrant, the map distribution shifts the mass to the right. (c) The robot then moves right and observes the actual hydrant.

approaching the performance of the system when it begins with a completely known map of the environment.

One interesting failure case is when the robot is instructed to "go to the hydrant nearest to the cone" in an environment with two hydrants. In instances where the robot sees a hydrant first, it hypothesizes the location of the cone, and then identifies the observed hydrants and hypothesized cones as being consistent with the command. Since the robot never actually confirms the existence of the cone in the real world, this results in the incorrect hydrant being labeled as the goal.

Multi-room navigation The second set of Monte Carlo experiments goes beyond object-based navigation and considers natural language direction-following in a larger environment modeled after a multi-room office building (the MIT Stata Center) that consists of a laboratory, multiple hallways, and a kitchen. We compare our framework against two baselines. The first baseline ("Known Map") considers the ideal case in which the world model is known a priori, employing our HDCG statistical language grounding model to infer the actions consistent with the route instruction. The second assumes no prior knowledge of the environment (as with our method), but does not use language to modify the map. Instead, the baseline uses our HDCG framework to opportunistically ground the command in the current semantic map generated from observations z^t (but not language). Note that, as with our framework, this baseline performs the grounding anew as the map evolves. We refer to this method as the "Without Language" baseline. Note that this and the "Known Map" baselines use an anytime RRT* planner (Karaman et al., 2011) to plan paths to the goal identified by language grounding.

Table 2: Simulation-based evaluation of natural language route direction-following.

	Distance (m)		Time (sec)	
Algorithm	Mean	Standard Deviation	Mean	Standard Deviation
Known Map	12.88	0.06	18.32	3.54
With Language (Ours)	16.64	6.84	82.78	10.56
Without Language	25.28	12.99	85.57	17.80

Table 2 compares the total distance traveled along with the execution time for the three methods, averaged over ten Monte Carlo simulations, along with the standard deviation. As expected, with access to the world model, the "Known Map" baseline has the robot navigate directly to the desired goal, achieving the shortest path and smallest execution time. In contrast, the "Without Language" baseline continues to ground the instructions in incomplete maps, often choosing to initially explore the second (incorrect) hallway, before opportunistically discovering the kitchen. This results in longer average paths (and higher standard deviation) as well as significantly higher execution times (also with higher standard deviation). By taking advantage of the environment knowledge implicit in the command, our method enables the robot to act more deliberately, reaching the intended goal along paths that are only slightly longer than those of the "Known Map" baseline. However, our framework does require significantly more time to follow the directions than the known map scenario. In part, this increase results from the robot stopping each time it reaches an intermediate goal selected by the policy, at which time the algorithm updates the semantic map distribution, grounds the instruction to a set of behaviors, and then evaluates the policy to identify the next action. In contrast, the robot navigates without stopping until it reaches the goal with the known map baseline. The additional computational requirements of our framework will inherently result in larger runtimes, however we note that a non-negligible fraction of the additional time is due to our implementation, which explicitly required the robot to pause for several seconds before moving on to the next waypoint.

5.1.2 Physical Experiments

We further evaluate our method through a series of experiments in which different robots were tasked with following natural language navigation instructions in a priori unknown environments. The first set of experiments emulates the aforementioned Monte Carlo experiments in which a Clearpath Husky A200 Unmanned Ground Vehicle (Fig. 7(a)) and a voice-commandable wheelchair (Fig. 7(b))[6] were instructed to navigate to an unknown object. As with the simulation-based experiments, these commands did not match those used to train our language grounding models.

Each experiment involves a variation in the number and position of various objects in the environment (namely, cones and hydrants), the command, as well as changes in the robot's field-of-view. Figure 11 shows one such experiment in which the Clearpath Husky robot is instructed to navigate to the hydrant behind

[6]The wheelchair employs a cloud-based speech recognizer to convert spoken instructions to text, which is then provided as input to our architecture. The platform also supports limited onboard recognition (Hetherington, 2007) in the event that the cloud-based recognizer is unavailable.

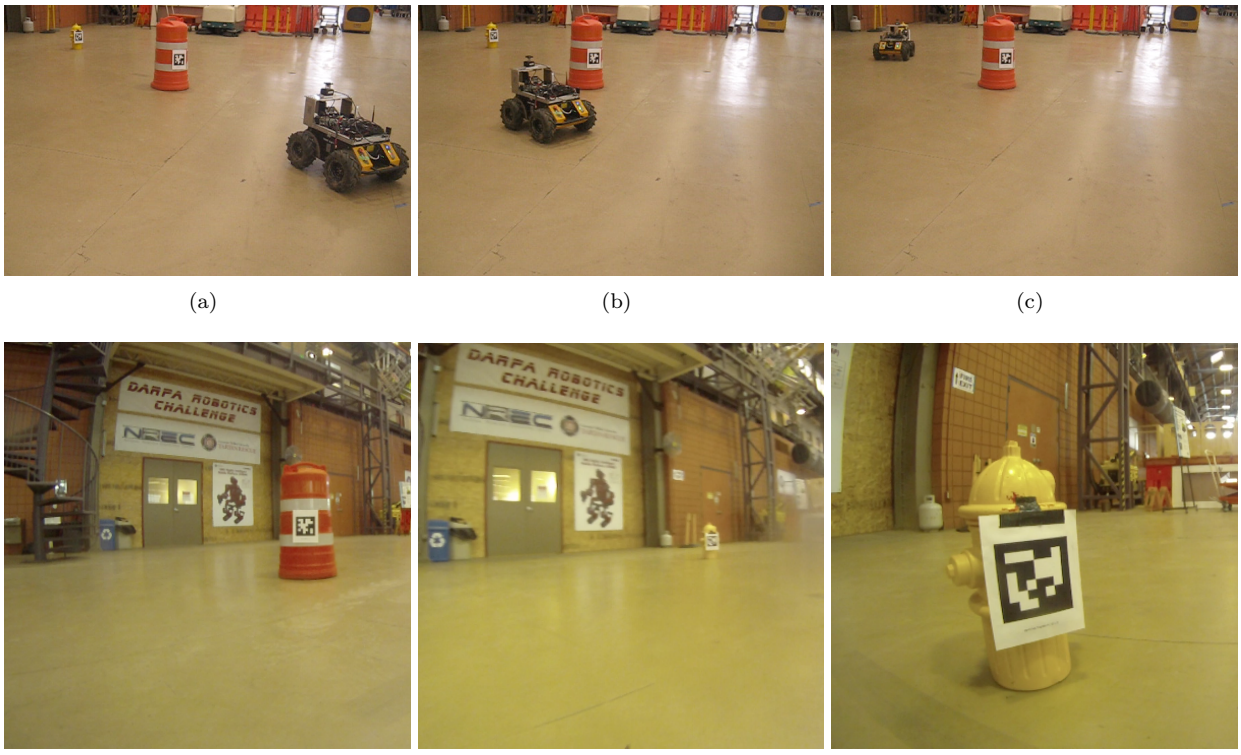

(a) (b) (c)

(d) (e) (f)

Figure 11: Third- (top) and first-person (bottom) perspectives of a Clearpath Robotics Husky A200 Unmanned Ground Vehicle responding to the command "navigate to the hydrant behind the barrel" in an a priori unknown environment. Subfigures (a) and (d) show the third- and first-person perspective when the robot receives the initial instruction. Note that the hydrant is not in view, so that object is not available for grounding in the baseline approach. Subfigures (b) and (e) followed by (c) and (f) show the robot as it navigates to a hypothesized hydrant behind the observed barrel. Once the hydrant becomes visible and is placed in the environment model, the distribution converges to the visually observed state.

the cone. Initially, only the cone is visible to the robot (Figs. 11(a) and 11(d)), at which point the algorithm hypothesizes the location of the hydrant. As the robot navigates according to the world model distribution, it detects the presence of a hydrant (Figs. 11(b) and 11(e)), and then drives straight to the goal (Figs. 11(c) and 11(f)). For each configuration of the environment, command, and field-of-view, we perform ten trials with our algorithm with the wheelchair and six with the Husky. As a baseline, we perform an additional run with a completely known world model. We consider a run to be a success when the robot's final destination is within 1.5 m of the intended goal.

Table 3: Wheelchair object-relative navigation experimental results with 1σ confidence intervals.

Environment		FOV (m)	Relation	Success Rate (%)		Distance (m)	
				Known	Ours	Known	Ours
1 hydrant	1 cone	2.5	null	100.0	100.0	4.69	16.56 (7.20)
1 hydrant	1 cone	2.5	"behind"	100.0	100.0	4.69	9.91 (3.41)
1 hydrant	2 cones	3.0	"behind"	100.0	100.0	4.58	7.64 (2.08)
2 hydrants	1 cone	2.5	"behind"	100.0	80.0	5.29	6.00 (1.38)
2 hydrants	1 cone	4.0	"nearest"	100.0	100.0	4.09	4.95 (0.39)
2 hydrants	1 cone	3.0	"nearest"	100.0	50.0	6.30	7.05 (0.58)

(a) Voice-commandable wheelchair

(b) Occupancy grid map of the environment

Figure 12: A (a) voice-commandable wheelchair was tasked with following natural language route instructions in (b) a 30 m × 30 m (approx.) office-like environment consisting of multiple hallways and rooms. The wheelchair employs a cloud-based speech recognizer to convert spoken instructions to text, which is then provided as input to our architecture. The platform also supports limited onboard recognition (Hetherington, 2007) in the event that the cloud-based recognizer is unavailable.

Table 3 presents the performance of our algorithm averaged over ten runs per scenario with the wheelchair, and compares against the baseline that has full knowledge of the environment. Experiments with the Husky demonstrate similar results with an average distance traveled of 8.1 m ($\sigma = 1.3$ m) with our method compared to 8.4 m ($\sigma = 0.6$ m) with the known map baseline and a success rate of 83.3% v.s. 100% with the baseline, based on six runs each. Together, the results demonstrate that our algorithm is able to take advantage of spatial relations that may be implicit in the instructions to identify more informed, deliberate paths to the goal. The ability to leverage information about spatial relations is important when there are multiple objects in the environment that match the figure in the instruction. For example, when there were two hydrants and the user commands the robot to "go to the hydrant behind the cone", the robot successfully identifies the correct hydrant as the goal in eight of the ten experiments. Similar to the failure discussed above for the simulation-based experiments, the two failures occur when the robot initially sees only the incorrect hydrant, upon which the semantic map hypothesizes the existence of cones in front of the hydrant. This results in a behavior distribution that is peaked around this goal. In the eight successful trials, the robot observes all three objects and infers the correct behavior. Similarly, if we consider the command "go to the hydrant nearest to the cone" we find that the robot reaches the goal in all ten experiments with a 4 m field-of-view. However, reducing the field-of-view to 3 m results in the robot reaching the goal in only half of the trials.

Next, we evaluate our framework on a mobile robot tasked with following natural language route instructions in an unknown environment. We implemented our architecture on a voice-commandable wheelchair (Fig. 12(a)) that is equipped with three forward-facing monocular cameras with a collective field-of-view of 120 degrees, and forward- and rearward-facing Hokuyo UTM LIDARs. The wheelchair was placed in a lobby within MIT's Stata Center, with several hallways, offices, and lab spaces, as well as a kitchen on the same floor. In an effort to facilitate perception, these experiments employed AprilTag fiducials (Olson, 2011) to identify the existence and semantic type of regions in the environment. We trained the HDCG models on a parallel corpus of 54 fully labeled examples. We then directed the wheelchair to execute the instruction "go to the kitchen that is down the hallway" that was not seen during training.

As with the previous experiments, we compare our framework with two baselines. The "Known Map" baseline emulates the previous state-of-the-art and uses a known map of the environment in order to infer the actions consistent with the route direction. The second "Without Language" baseline assumes no prior knowledge of the environment (as with ours) and opportunistically grounds the command in the map, but does not use language to modify the map. We performed six experiments with our algorithm, three with

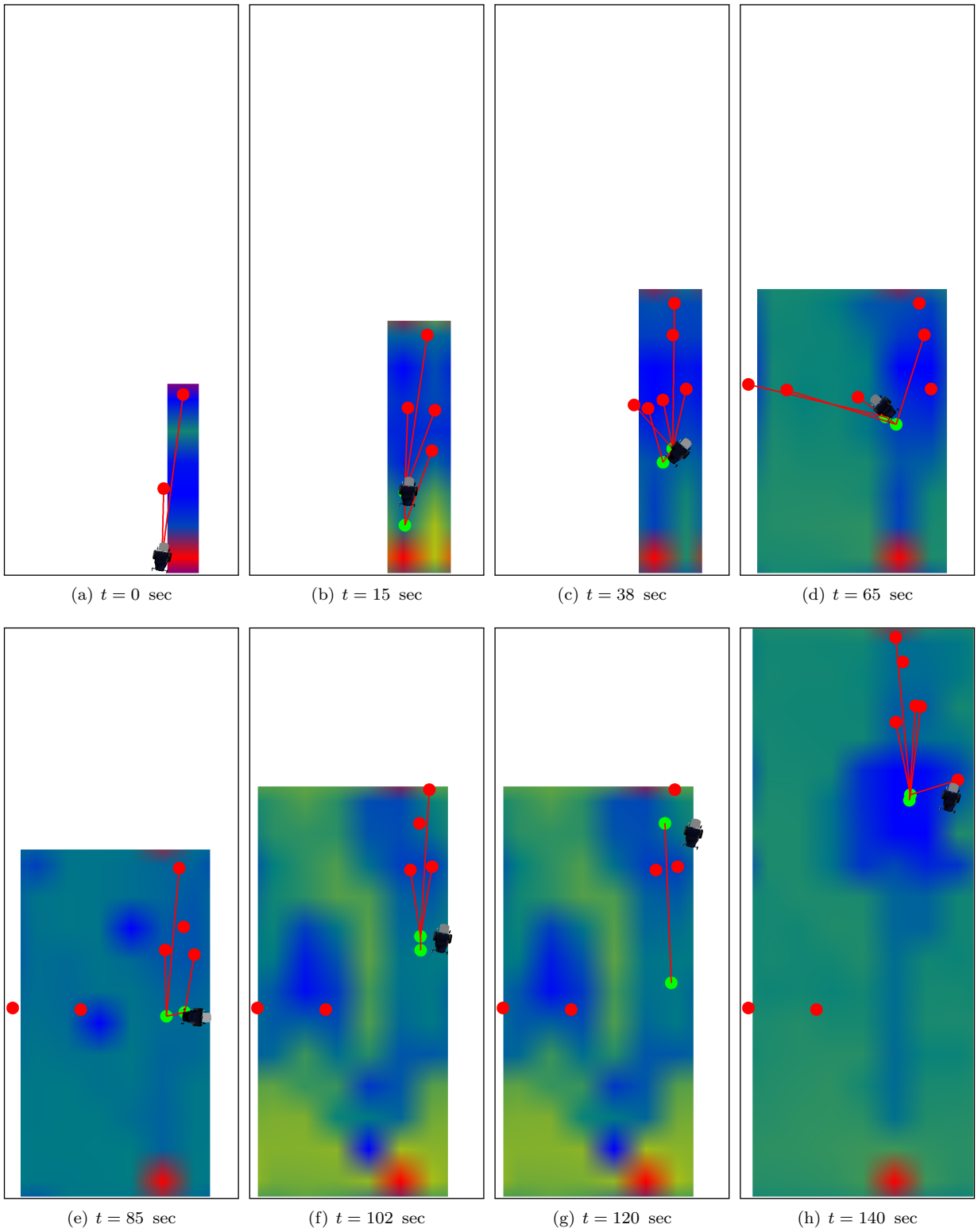

(a) $t = 0$ sec (b) $t = 15$ sec (c) $t = 38$ sec (d) $t = 65$ sec

(e) $t = 85$ sec (f) $t = 102$ sec (g) $t = 120$ sec (h) $t = 140$ sec

Figure 13: The evolution of the planner cost function for the command "go to the kitchen that is down the hallway". Red nodes indicate candidate destinations and green nodes indicate previously visited locations. The normalized cost function is rendered using the colormap:  , where blue and red denote costs of 0 and 1, respectively. The planner (d) initially directs the robot down the wrong hallway, but after not seeing the hypothesized kitchen, (f) the robot navigates down the correct hallway (h) to the goal.

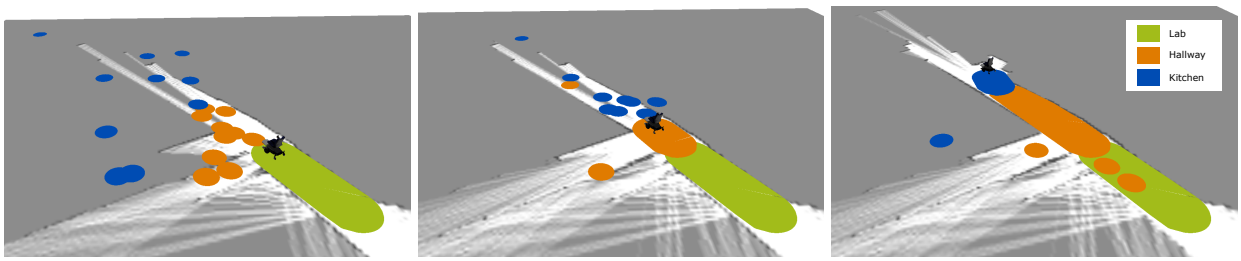

Figure 14: A visualization that shows how the semantic map evolves time as the robot follows the command "go to the kitchen that is down the hallway." Small circles and large filled-in areas denote sampled and visited regions, respectively, each colored according to its class type. The robot (left) first samples possible locations of the kitchen and moves towards them, (middle) then observes the hallway and refines its estimate using the "down" relation provided by the user. Finally, the robot (right) reaches the actual kitchen and declares it has finished following the direction.

the known map method, and five with the method that does not use language for environment inference, all of which were successful (the robot reached the kitchen). Figure 13 visualizes the evolution of the planner's cost function for one of the experiments. The cost, which is a function of the semantic map distribution and the inferred behavior(s), initially suggests that the wheelchair navigate down the wrong hallway (Fig. 13(d)), but after not observing the kitchen, the map updates and the planner later leads the robot to the correct goal. Figure 14 shows a visualization of the semantic maps over several time steps for one successful run on the robot.

Table 4: Evaluation of natural language route direction-following with the wheelchair.

	Distance (m)		Time (sec)	
Algorithm	Mean	Standard Deviation	Mean	Standard Deviation
Known Map	13.10	0.67	62.48	16.61
With Language	12.62	0.62	122.14	32.48
Without Language	24.91	13.55	210.35	97.73

Table 4 compares the total distance traveled and execution time for the three methods. Our algorithm resulted in paths with lengths close to those of the known map, and significantly outperformed the method that did not use language for mapping. As with the Monte Carlo simulations, our framework required significantly more time to follow the directions than the known map baseline. Some of this additional time results from the robot stopping each time it reaches an intermediate goal selected by the policy (in contrast to the known map baseline, which does not stop until it reaches the goal) at which time the algorithm updates the semantic map distribution, grounds the instruction to a set of behaviors, evaluates the policy to identify the next action, and then performs motion planning. While this will inherently result in larger runtimes compared to the known map setting, we note that a non-negligible fraction of the additional time (nearly half in some cases) is due to our implementation, which explicitly required the robot to pause for several seconds before moving on to the next waypoint.

5.2 Instruction Following for Mobile Manipulation

Having evaluated the performance of the proposed model through simulated experiments and in the real world by using fiducial based perception, we now expand upon our analysis by involving non-fiducial based perception, which is computationally more expensive and often not as accurate as fiducial-based perception. To analyze the runtime performance of the proposed framework for mobile manipulation tasks, we implemented the architecture on a Clearpath Husky A200 Unmanned Ground Vehicle fitted with a Universal Robotics UR5 arm and Robotiq 3-Finger Adaptive Robot Gripper 7(c). Image data for visual perception was captured using an Intel RealSense RGB-D sensor mounted on the wrist of the UR5 arm. The perception

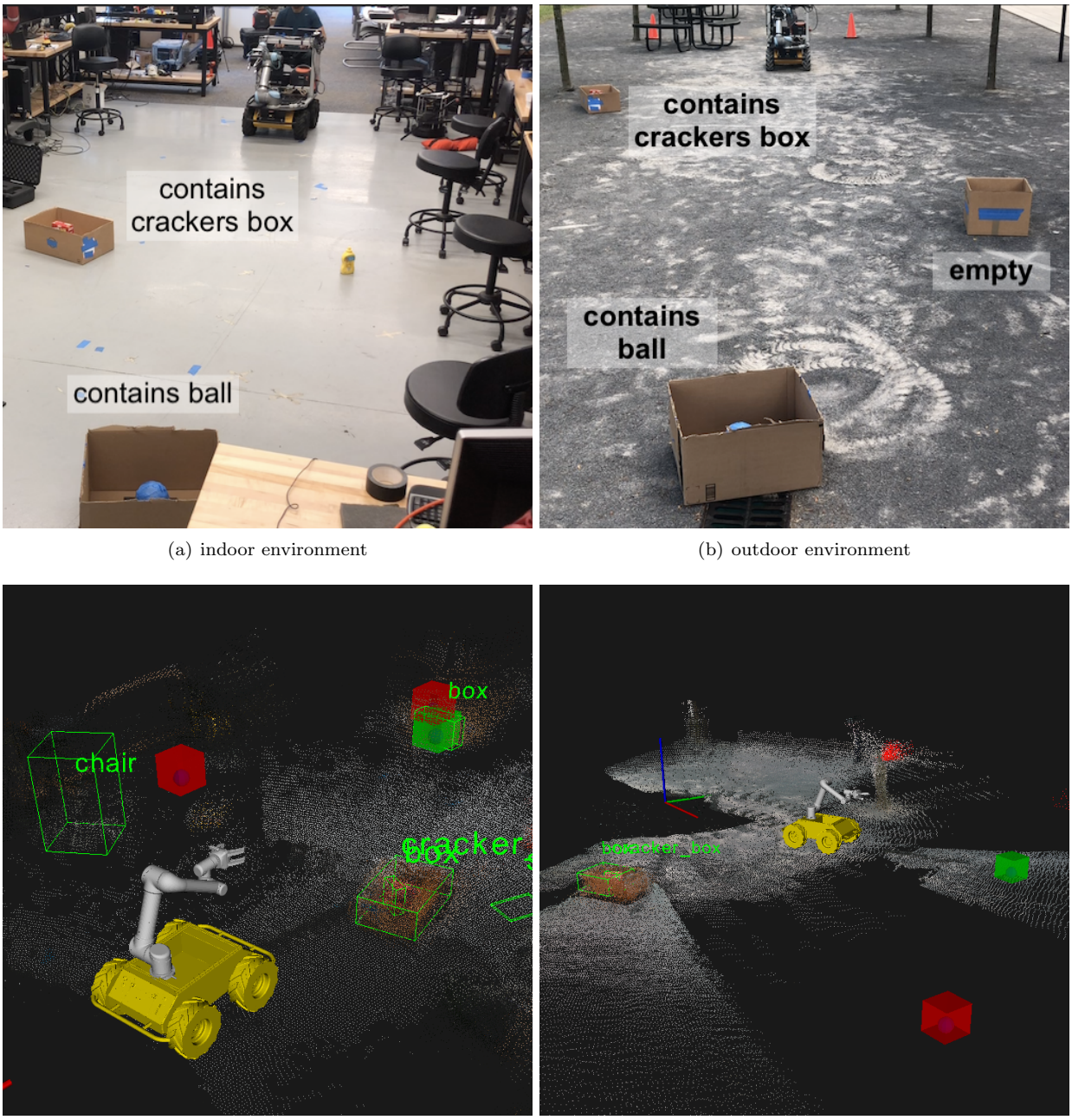

(a) indoor environment

(b) outdoor environment

(c) indoor map at $t = 57\,\text{sec}$

(d) outdoor map at $t = 177\,\text{sec}$

Figure 15: The mobile manipulation experiments involved placing the arm-equipped Husky in a priori unknown (a) indoor and (b) outdoor environments with several boxes that contained different or no objects. The robot was then given a natural language instruction to retrieve a specific object from a box. Without any prior knowledge of the environment, the robot initially navigates towards a hypothesized box (rendered as solid red cubes in the bottom figures). Upon detecting a box, the robot updates the world model distribution and then explores the nearest observed box (a green wireframe denotes objects that the robot has observed), which does not contain the object of interest. At this point, the robot either (c) explores the next box that comes within the robot's field-of-view (for the indoor experiments), or (d) continues to explore the environment (for the outdoor experiments) as guided by the maintained world distribution.

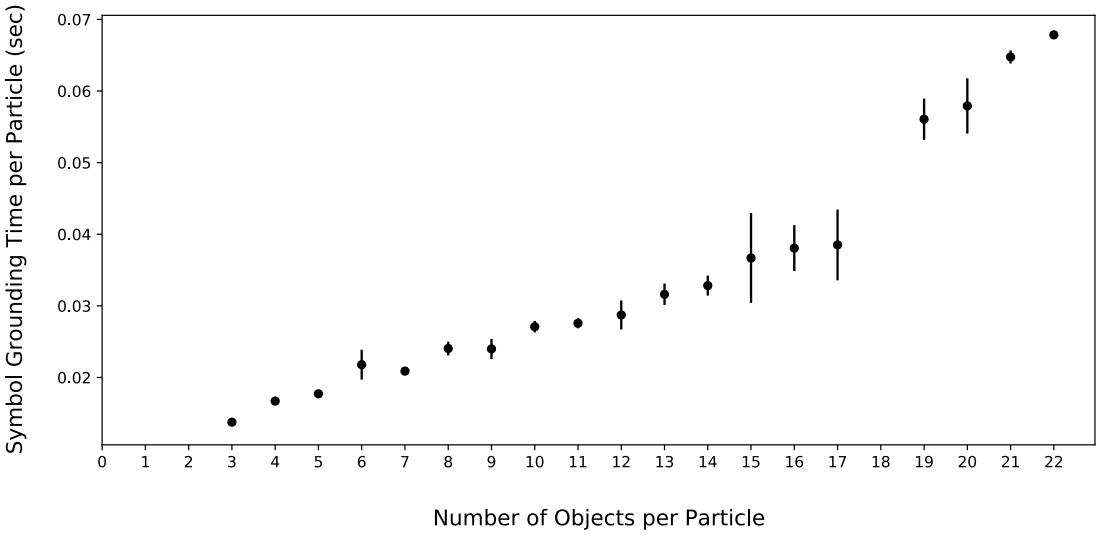

Figure 16: A graph that shows the increase in symbol grounding runtime per particle as a function of an increase in the number of detected objects in the particle.

pipeline consisted of multiple custom-trained YOLO-V3 (Redmon and Farhadi, 2018) detectors. Specifically, we used a full YOLO-V3 model trained on the COCO (Lin et al., 2014) dataset and 15 tiny YOLO-V3 models trained on individual classes from the YCB (Calli et al., 2015) and OpenImages-V4 (Kuznetsova et al., 2018) datasets. We projected the 2D image-space bounding boxes generated by the YOLO-V3 detectors to the aligned 3D point clouds in order to obtain metric information about the objects in the robot's environment. Associated with each detected object was its semantic label generated by YOLO-V3 detector, a six degree-of-freedom pose estimate, and a 3D collision geometry represented by an oriented bounding box. The range of sensing was restricted to 4.5 m indoors and 7.0 m outdoors to eliminate noisy point cloud data.

Figure 15 illustrates the workspace setup for both indoor and outdoor environments. In both environments, the robot was initially instructed to "retrieve the ball inside the box". The indoor experiment followed with a second command to "pick up the crackers box inside the box", whereas the outdoor experiment followed with "go to the crackers box". In both of the settings, the box containing the ball was past the sensing horizon of the robot at the start, while the box containing the crackers box was observable. The workspace in the indoor environment was set up such that the robot will most likely detect and check the second box after inspecting the closer box and finding it empty. The larger workspace in the outdoor experiment allowed us to set up boxes far away from each other so that the robot would need to explore the environment using the hypothesized distribution to eventually reach the goal location. In order to build accurate models of the environment, a speed of 0.3 m per perception cycle chosen for these experiments. We used 10 particles to represent the distribution over world models in the indoor experiment, while we used 20 particles for the outdoor experiment to account for the larger environment.

We developed and deployed a motion planner capable of performing manipulation actions that used TRAC-IK (Beeson and Ames, 2015) for inverse kinematics. The architecture guided the robot to perform the most likely action identified through behavior inference. Upon reaching a box, the arm was positioned to look inside it. If this observation conveyed the absence of the object of interest, the robot would back up, pan the camera ± 30 deg, and navigate towards a new goal selected from the updated distribution. If the desired object defined by the selected goal was observed in the box, the robot would execute the remaining activities to complete its inferred action.

We analyzed the runtime of task execution by measuring the individual runtimes of perception and behavior inference as outlined in Table 5. Figures 17 and 18 shows the state of the robot while executing the instruction. The robot took approximately six minutes to execute the first task in the indoor environment, while requiring approximately ten minutes for the outdoor experiments. Such long task execution runtimes are undesirable for fluent human-robot collaboration. As observed in Table 5, a large fraction of the task

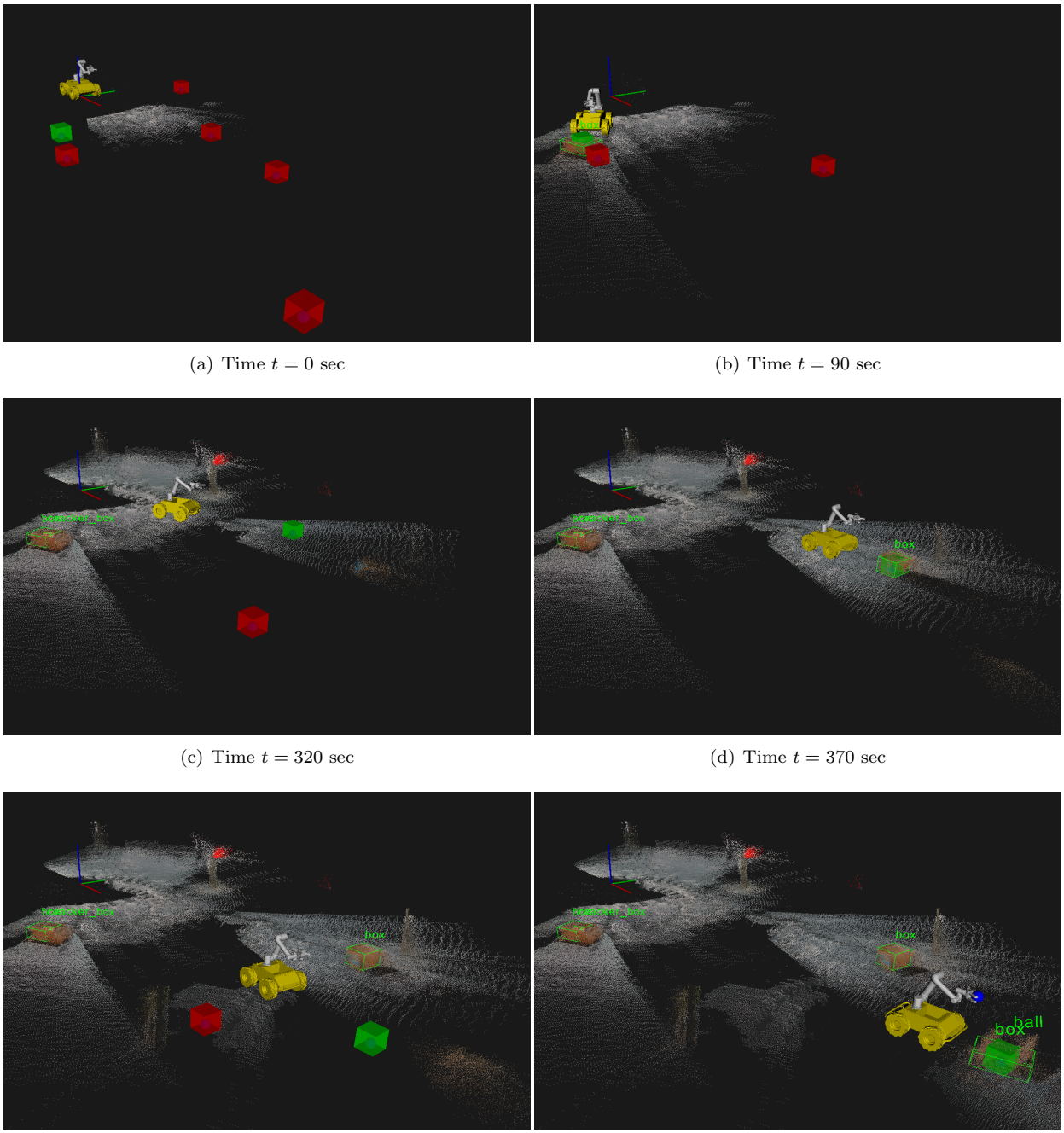

(a) Time $t = 0$ sec

(b) Time $t = 90$ sec

(c) Time $t = 320$ sec

(d) Time $t = 370$ sec

(e) Time $t = 500$ sec

(f) Time $t = 563$ sec

Figure 17: Visualization of the state of the robot while executing the instruction "retrieve the ball inside the box" in the outdoor environment. In (a) we visualize the hypothesized locations of boxes (in red), each containing a ball, sampled from the world model distribution that our algorithm maintains. The solid green cube denotes the hypothesized box that is the current goal of the planner. The robot then (b) detects an actual box and looks inside it to find that it does not contain a ball. As (c) the robot navigates to a hypothesized box, it (d) detects actual boxes that are found to not contain a ball, while also failing to confirm the presence of hypothesized boxes sampled from the distribution. The algorithm (e) updates the world model distribution accordingly, and the planner updates the goal. This continues until (f) the robot observes a box containing a ball and subsequently retrieves the ball, satisfying the instruction.

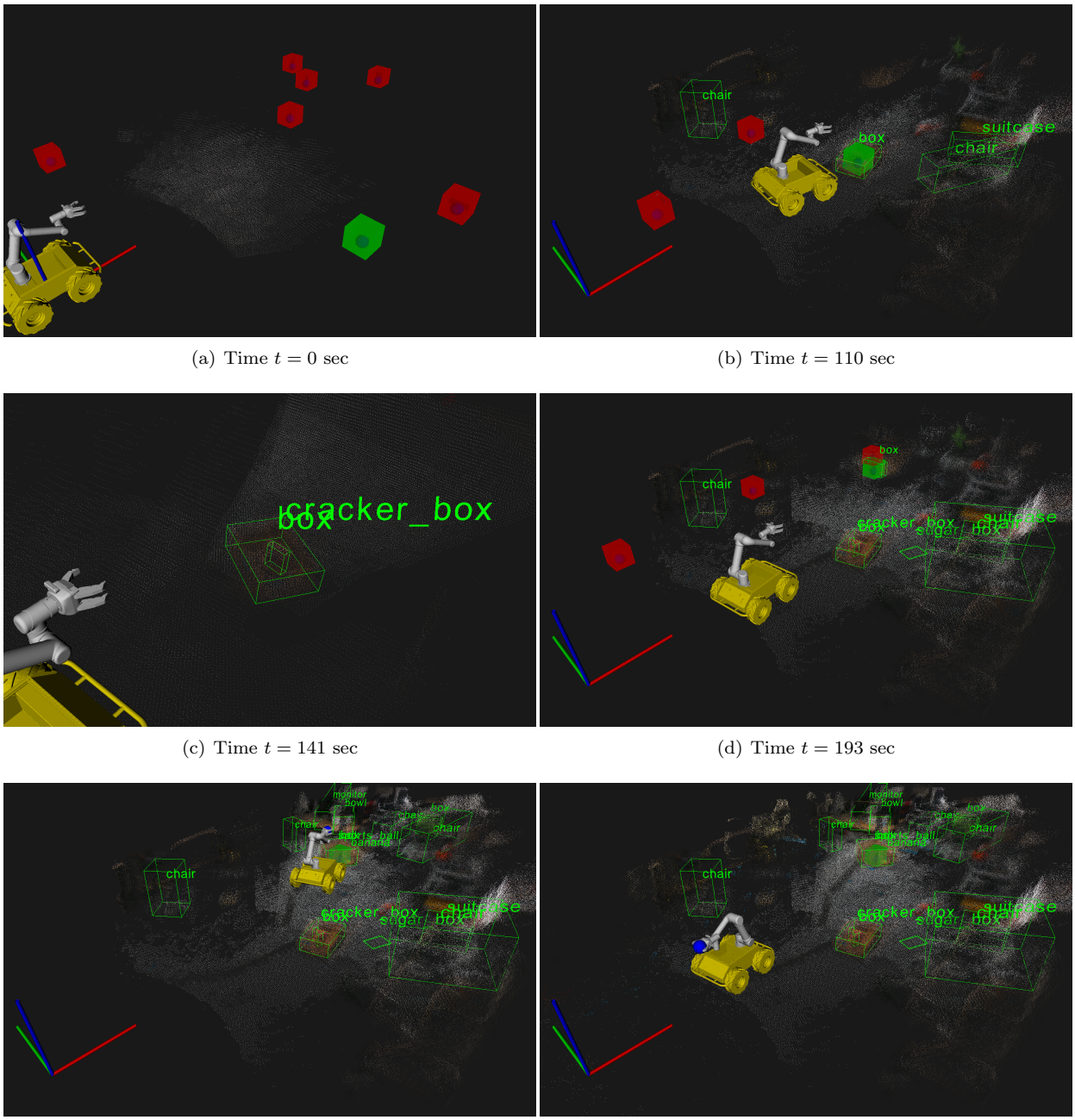

(a) Time $t = 0$ sec

(b) Time $t = 110$ sec

(c) Time $t = 141$ sec

(d) Time $t = 193$ sec

(e) Time $t = 310$ sec

(f) Time $t = 346$ sec

Figure 18: Visualization of the state of the robot while executing the instruction "retrieve the ball inside the box" in the indoor environment. In (a) we visualize the hypothesized locations of boxes (in red), each containing a ball, sampled from the world model distribution that our algorithm maintains. The solid green cube denotes the hypothesized box that is the current goal of the planner. The robot then detects an actual box (b) and looks inside it to find (c) that it does not contain a ball, but instead contains a crackers box. The robot (d) eventually detects the second box. The algorithm updates the world model distribution accordingly, and the planner updates the goal. The robot (e) observes a box containing a ball and subsequently (f) retrieves the ball, satisfying the instruction.

Table 5: Perception and symbol grounding runtime analysis for indoor and outdoor trials (three each).

	Indoor	Outdoor
average behavior inference runtime per particle (seconds)	0.035 ± 0.01	0.019 ± 0.002
average perception cycle runtime (seconds)	4.141 ± 0.11	4.099 ± 0.060
first task runtime (seconds)	351.2	593.5
second task runtime (seconds)	149.5	20.4
total number of detected objects	24	11
total number of perception cycles during first task	69	127
total number perception cycles during second task	27	3

execution runtime was spent on perception, building a rich model of the robot's environment such as the one in Figure 18(f). Such high fidelity world models are computationally expensive to build and are also unnecessarily detailed for grounding, planning, and executing the instructed task. This raises open questions regarding how to optimally perceive the robot's world for collaborative robots which are required to understand and execute a diverse set of instructions. Furthermore, Figure 16 indicates a positive correlation between the symbol grounding runtime per particle and the number of objects present in the particle (i.e., the fidelity of the world model). This means that maintaining a distribution over highly detailed world models and reasoning in its context is computationally expensive in terms of both perception and symbol grounding. We elaborate on this issue and possible ways to improve scalability below.

6 Discussion

As established through the experimental evaluation in simulation and on actual robots, the proposed model enables natural-language instruction-following in previously unseen or partially observed environments. It provides a guided and efficient exploration mechanism that allows faster runtimes for task execution in previously unseen environments as compared to the baseline of opportunistic exploration. However, we note that the spatial extent of the environments considered in the experimental evaluation is small compared to those of typical field and service robotics settings. While we have previously demonstrated the ability to learn maps of larger, multi-building environments from human-provided descriptions (Walter et al., 2014), evaluating the proposed framework at this scale remains as future work.

As the experiments demonstrate, maintaining a distribution of highly-detailed world models and reasoning in its context is computationally expensive in terms of both perception and symbol grounding. Addressing this scalability challenge, a recent line of work (Patki and Howard, 2018; Patki et al., 2019, 2020) proposes learning to adapt the robot's perception pipeline by exploiting implied utterance information to construct task-relevant world models. These more compact, task-relevant world models afford faster perception and symbol-grounding runtimes, as compared to a baseline configuration that uses a non-adaptive and flat perception pipeline. Recent work (Patki et al., 2020) demonstrates approximately a 50% reduction in task-execution runtimes in both indoor and outdoor experiments, and illustrates the performance gains that can be achieved by incorporating our proposed adaptive-perception framework. Learning to constrain the robot's perception pipeline adaptively shortens the perception runtime by obviating irrelevant detectors. This reduction in the perception runtime enables our framework to operate more efficiently, while processing the same number of observations, and so reduces overall task-execution time. Furthermore, as behavior inference is performed on each hypothesized world model in the distribution, the efficiency gains provided by adaptive perception enables reasoning over a larger number of environment hypotheses in the same amount of time. This important ability allows maintaining more particles and thus to more efficiently explore previously unseen environments. As part of ongoing work, we are investigating the ability to extend our framework such that it is scalable to larger environments than those considered here.

Another limitation of the current approach is the reliance on fully-annotated data. Densely labeling examples for both annotation and behavior inference with different symbolic representations is a nontrivial task that involves inferring the presence of relationships needed to perform grounding in a space of hypothesized worlds. Approaches that are amenable to partially-annotated data, e.g., by using the available annotations to

learn how to automatically label the rest of the dataset, would significantly facilitate integrating annotation- and behavior-inference and enable robots to learn models for both processes in situ. A human operator attempting to demonstrate the concept "pick up the cup on the table" would have to group physical objects "cup" and "table," along with the spatial relation represented by the phrase "on" for behavior inference, and also associate the physical relationship between two hypothesized objects with their associated semantic labels to properly capture this information for annotation inference. Algorithms capable of this remain an open area of investigation.

Another deficiency of this approach is that the procedures for both annotation and behavior inference does not express bounds on the space of worlds or language wherein the expressed symbols would remain valid. Uncertainty in automatic speech-recognition and parsing could influence the quality of annotation inference, and behavior inference could further be impacted by noise in perception. More efficient and effective methods for evaluating confidence in an expressed set of symbols may influence whether the robot should exploit these annotations or engage in dialogue with a human to confirm that such information should be added to the environment model.

7 Conclusions

Significant progress in grounded natural-language understanding has enabled robots to interpret a diverse array of free-form navigation, manipulation, and mobile-manipulation commands. However, most contemporary approaches require a pre-existing, detailed spatial-semantic map of the robot's environment that represents the objects or regions that the utterance may reference. Consequently, these methods fail when robots are deployed in previously unseen or partially-observed environments, particularly when mental models of the environment differ between the human user and robot. This paper describes a learning framework that allows field and service robots to execute natural-language instructions in previously unseen or partially-observed environments. The experimental results in simulation and on three different robotic platforms indicate that the proposed model facilitates faster task execution in previously unseen environments as compared to a contemporary language-grounding baseline that does not take advantage of environment information available in the instruction. The results also show that the method is amenable to tasks that include navigation and mobile manipulation. Importantly, experimental data also reveal limitations of the approach, including the challenge of maintaining a distribution over highly-detailed world models and reasoning in its context, which is computationally expensive in terms of both perception and symbol grounding. This observation raises interesting, open-ended questions that are the focus on ongoing research, such as how to represent complex environments efficiently while also supporting a diverse array of tasks in large-scale environments.

8 Acknowledgements

This work was supported in part by the National Science Foundation under grants IIS-1638072 and IIS-1637813, by the Robotics Consortium of the U.S. Army Research Laboratory under the Collaborative Technology Alliance Program Cooperative Agreement W911NF-10-2-0016, and by ARO grants W911NF-15-1-0402 and W911NF-17-1-0188.

References

Abbeel, P. and Ng, A. Y. (2004). Apprenticeship learning via inverse reinforcement learning. In *Proceedings of the International Conference on Machine Learning (ICML)*.

Anderson, P., Wu, Q., Teney, D., Bruce, J., Johnson, M., Sünderhauf, N., Reid, I., Gould, S., and van den Hengel, A. (2018). Vision-and-language navigation: Interpreting visually-grounded navigation instructions in real environments. In *Proceedings of the IEEE Conference on Computer Vision and Pattern Recognition (CVPR)*, pages 3674–3683.

Arkin, J., Park, D., Roy, S., Walter, M. R., Roy, N., Howard, T. M., and Paul, R. (2020). Multimodal

estimation and communication of latent semantic knowledge for robust execution of robot instructions. *International Journal of Robotics Research*, 39(10–11):1279–1304.

Arkin, J., Paul, R., Park, D., Roy, S., Roy, N., and Howard, T. M. (2018). Real-time human-robot communication for manipulation tasks in partially observed environments. In *Proceedings of the International Symposium on Experimental Robotics (ISER)*, pages 448–460.

Arvidson, R. E., Bell, J., Bellutta, P., Cabrol, N. A., Catalano, J., Cohen, J., Crumpler, L. S., Des Marais, D., Estlin, T., Farrand, W., et al. (2010). Spirit Mars Rover Mission: Overview and selected results from the northern Home Plate Winter Haven to the side of Scamander crater. *Journal of Geophysical Research: Planets*, 115(E7).

Aydemir, A., Pronobis, A., Göbelbecker, M., and Jensfelt, P. (2013). Active visual object search in unknown environments using uncertain semantics. *IEEE Transactions on Robotics*, 29(4):986–1002.

Aydemir, A., Sjöö, K., Folkesson, J., Pronobis, A., and Jensfelt, P. (2011). Search in the real world: Active visual object search based on spatial relations. In *Proceedings of the IEEE International Conference on Robotics and Automation (ICRA)*, pages 2818–2824.

Bacha, A., Bauman, C., Faruque, R., Fleming, M., Terwelp, C., Reinholtz, C., Hong, D., Wicks, A., Alberi, T., Anderson, D., Cacciola, S., Currier, P., Dalton, A., Farmer, J., Hurdus, J., Kimmel, S., King, P., Taylor, A., Covern, D. V., and Webster, M. (2008). Odin: Team VictorTango's entry in the DARPA Urban Challenge. *Journal of Field Robotics*, 25(8):467–492.

Bansal, S., Tolani, V., Gupta, S., Malik, J., and Tomlin, C. (2019). Combining optimal control and learning for visual navigation in novel environments. In *Proceedings of the Conference on Robot Learning (CoRL)*, pages 420–429.

Barber, D., Howard, T. M., and Walter, M. (2016). A multimodal interface for real-time soldier-robot teaming. In *Unmanned Systems Technology XVIII*, volume 9837. International Society for Optics and Photonics.

Beeson, P. and Ames, B. (2015). TRAC-IK: An open-source library for improved solving of generic inverse kinematics. In *Proceedings of the IEEE-RAS International Conference on Humanoid Robots (Humanoids)*, pages 928–935.

Blanco, J.-L., Gonzalez, J., and Fernandez-Madrigal, J. (2006). Consistent observation grouping for generating metric-topological maps that improves robot localization. In *Proceedings of the IEEE International Conference on Robotics and Automation (ICRA)*, pages 818–823.

Bohren, J., Foote, T., Keller, J., Kushleyev, A., Lee, D., Stewart, A., Vernaza, P., Derenick, J., Spletzer, J., and Satterfield, B. (2008). Little Ben: The Ben Franklin Racing Team's entry in the 2007 DARPA Urban Challenge. *Journal of Field Robotics*, 25(9):598–614.

Bollini, M., Tellex, S., Thompson, T., Roy, N., and Rus, D. (2010). Interpreting and executing recipes with a cooking robot. In *Proceedings of the International Symposium on Experimental Robotics (ISER)*, pages 481–495.

Boteanu, A., Arkin, J., Howard, T. M., and Kress-Gazit, H. (2016). A model for verifiable grounding and execution of complex language instructions. In *2016 IEEE/RSJ International Conference on Intelligent Robots and Systems*, pages 2649–2654.

Bowen, A. D., Yoerger, D. R., Taylor, C., McCabe, R., Howland, J., Gomez-Ibanez, D., Kinsey, J. C., Heintz, M., McDonald, G., Peters, D. B., et al. (2008). The Nereus hybrid underwater robotic vehicle for global ocean science operations to 11,000 m depth. In *Proceedings of the IEEE/MTS OCEANS Conference and Exhibition*.

Broad, A., Arkin, J., Ratliff, N., Howard, T. M., and Argall, B. (2017). Real-time natural language corrections for assistive robotic manipulators. *International Journal of Robotics Research*, 36(5-7):684–698.

Calli, B., Walsman, A., Singh, A., Srinivasa, S., Abbeel, P., and Dollar, A. M. (2015). Benchmarking in manipulation research: The YCB object and model set and benchmarking protocols. *IEEE Robotics and Automation Magazine*, pages 36–52.

Camilli, R., Reddy, C. M., Yoerger, D. R., Van Mooy, B. A., Jakuba, M. V., Kinsey, J. C., McIntyre, C. P., Sylva, S. P., and Maloney, J. V. (2010). Tracking hydrocarbon plume transport and biodegradation at Deepwater Horizon. *Science*, 330(6001):201–204.

Chen, D. L. and Mooney, R. J. (2011). Learning to interpret natural language navigation instructions from observations. In *Proceedings of the National Conference on Artificial Intelligence (AAAI)*, pages 859–865.

Chiang, H.-T. L., Faust, A., Fiser, M., and Francis, A. (2019). Learning navigation behaviors end-to-end with AutoRL. *IEEE Robotics and Automation Letters*, 4(2):2007–2014.

Chung, I., Propp, O., Walter, M., and Howard, T. (2015). On the performance of hierarchical distributed correspondence graphs for efficient symbol grounding of robot instructions. In *Proceedings of the IEEE/RSJ International Conference on Intelligent Robots and Systems (IROS)*, pages 5247–5252.

Crammer, K. and Singer, Y. (2002). On the algorithmic implementation of multiclass kernel-based vector machines. *Journal of Machine Learning Research*, 2:265–292.

Daniele, A. F., Bansal, M., and Walter, M. R. (2017). Navigational instruction generation as inverse reinforcement learning with neural machine translation. In *Proceedings of the ACM/IEEE International Conference on Human-Robot Interaction (HRI)*, pages 109–118.

Doucet, A. (1998). On sequential simulation-based methods for bayesian filtering. Technical Report CUED/F-INFENG/TR 310, Department of Engineering, University of Cambridge.

Doucet, A., de Freitas, N., Murphy, K., and Russell, S. (2000). Rao-Blackwellised particle filtering for dynamic Bayesian networks. In *Proceedings of the Conference on Uncertainty in Artificial Intelligence (UAI)*, pages 176–183.

Duff, E. S., Roberts, J. M., and Corke, P. I. (2003). Automation of an underground mining vehicle using reactive navigation and opportunistic localization. In *Proceedings of the IEEE/RSJ International Conference on Intelligent Robots and Systems (IROS)*, pages 3775–3780.

Durrant-Whyte, H., Pagac, D., Rogers, B., Stevens, M., and Nelmes, G. (2007). Field and service applications—an autonomous straddle carrier for movement of shipping containers—from research to operational autonomous systems. *IEEE Robotics & Automation Magazine*, 14(3):14–23.

Durrant-Whyte, H. F. (1996). An autonomous guided vehicle for cargo handling applications. *International Journal of Robotics Research*, 15(5):407–440.

Duvallet, F., Kollar, T., and Stentz, A. (2013). Imitation learning for natural language direction following through unknown environments. In *Proceedings of the IEEE International Conference on Robotics and Automation (ICRA)*, pages 1047–1053.

Duvallet, F., Walter, M. R., Howard, T., Hemachandra, S., Oh, J., Teller, S., Roy, N., and Stentz, A. (2014). Inferring maps and behaviors from natural language instructions. In *Proceedings of the International Symposium on Experimental Robotics (ISER)*.

Eustice, R., Singh, H., and Leonard, J. (2005). Exactly sparse delayed-state filters. In *Proceedings of the IEEE International Conference on Robotics and Automation (ICRA)*, pages 2417–2424.

Furgale, P. and Barfoot, T. D. (2010). Visual teach and repeat for long-range rover autonomy. *Journal of Field Robotics*, 27(5):534–560.

Galindo, C., Saffiotti, A., Coradeschi, S., Buschka, P., Fernandez-Madrigal, J., and Gonzalez, J. (2005). Multi-hierarchical semantic maps for mobile robotics. In *Proceedings of the IEEE/RSJ International Conference on Intelligent Robots and Systems (IROS)*, pages 2278–2283.

German, C. R., Yoerger, D. R., Jakuba, M., Shank, T. M., Langmuir, C. H., and Nakamura, K.-i. (2008). Hydrothermal exploration with the Autonomous Benthic Explorer. *Deep Sea Research Part I: Oceanographic Research Papers*, 55(2):203–219.

Gong, Z. and Zhang, Y. (2018). Temporal spatial inverse semantics for robots communicating with humans. In *Proc. IEEE Int'l Conf. on Robotics and Automation (ICRA)*.

Gretton, A., Borgwardt, K., Rasch, M., Schölkopf, B., and Smola, A. J. (2007). A kernel method for the two-sample-problem. In *Advances in Neural Information Processing Systems (NeurIPS)*, pages 513–520.

Gupta, S., Davidson, J., Levine, S., Sukthankar, R., and Malik, J. (2017). Cognitive mapping and planning for visual navigation. In *Proceedings of the IEEE Conference on Computer Vision and Pattern Recognition (CVPR)*, pages 2616–2625.

Harnad, S. (1990). The symbol grounding problem. *Physica D*, 42:335–346.

Hemachandra, S., Duvallet, F., Howard, T. M., Roy, N., Stentz, A., and Walter, M. R. (2015). Learning models for following natural language directions in unknown environments. In *Proceedings of the IEEE International Conference on Robotics and Automation (ICRA)*, pages 5608–5615.

Hemachandra, S., Kollar, T., Roy, N., and Teller, S. (2011). Following and interpreting narrated guided tours. In *Proceedings of the IEEE International Conference on Robotics and Automation (ICRA)*, pages 2574–2579.

Hemachandra, S., Walter, M. R., Tellex, S., and Teller, S. (2014). Learning spatial-semantic representations from natural language descriptions and scene classifications. In *Proceedings of the IEEE International Conference on Robotics and Automation (ICRA)*, pages 2623–2630.

Hetherington, I. L. (2007). PocketSUMMIT: Small-footprint continuous speech recognition. In *Proceedings of Annual Conference of the International Speech Communication Association (INTERSPEECH)*, pages 1465–1468.

Howard, T., Chung, I., Propp, O., Walter, M., and Roy, N. (2014a). Efficient natural language interfaces for assistive robots. In *Proceedings of the IEEE/RSJ International Conference on Intelligent Robots and Systems (IROS) Workshop on Rehabilitation and Assistive Robotics*.

Howard, T. M., Tellex, S., and Roy, N. (2014b). A natural language planner interface for mobile manipulators. In *Proceedings of the IEEE International Conference on Robotics and Automation (ICRA)*, pages 6652–6659.

Johnson-Roberson, M., Pizarro, O., Williams, S. B., and Mahon, I. (2010). Generation and visualization of large-scale three-dimensional reconstructions from underwater robotic surveys. *Journal of Field Robotics*, 27(1):21–51.

Kaess, M., Ranganathan, A., and Dellaert, F. (2008). iSAM: Incremental smoothing and mapping. *Transactions on Robotics*, 24(6):1365–1378.

Kaess, M., Ranganathan, A., and Dellaert, F. (2009). iSAM: Incremental smoothing and mapping. http://people.csail.mit.edu/kaess/isam/.

Kang, S., Cho, C., Lee, J., Ryu, D., Park, C., Shin, K.-C., and Kim, M. (2003). ROBHAZ-DT2: Design and integration of passive double tracked mobile manipulator system for explosive ordnance disposal. In *Proceedings of the IEEE/RSJ International Conference on Intelligent Robots and Systems (IROS)*, pages 2624–2629.

Karaman, S., Walter, M. R., Perez, A., Frazzoli, E., and Teller, S. (2011). Anytime motion planning using the RRT*. In *Proceedings of the IEEE International Conference on Robotics and Automation (ICRA)*, pages 1478–1483.

Keiji, N., Swiga, K., Yoshito, O., et al. (2011). Redesign of rescue mobile robot Quince—Toward emergency response to the nuclear accident at Fukushima Daiichi Nuclear Power Station on March 2011. In *Proceedings of the IEEE International Symposium on Safety, Security, and Rescue Robotics (SSRR)*, pages 13–18.

Kim, D. K. and Chen, T. (2015). Deep neural network for real-time autonomous indoor navigation. *arXiv preprint arXiv:1511.04668*.

Kollar, T. and Roy, N. (2009). Utilizing object-object and object-scene context when planning to find things. In *Proceedings of the IEEE International Conference on Robotics and Automation (ICRA)*, pages 4116–4121.

Kollar, T., Tellex, S., Roy, D., and Roy, N. (2010). Toward understanding natural language directions. In *Proceedings of the ACM/IEEE International Conference on Human-Robot Interaction (HRI)*, pages 259–266.

Krieg-Brückher, B., Frese, U., Lüttich, K., Mandel, C., Massakowski, T., and Ross, R. J. (2005). Specification of an ontology for route graphs. *Spatial Cognition IV: Reasoning, Action, Interaction*, 3343:390–412.

Kuznetsova, A., Rom, H., Alldrin, N., Uijlings, J., Krasin, I., Pont-Tuset, J., Kamali, S., Popov, S., Malloci, M., Duerig, T., and Ferrari, V. (2018). The Open Images Dataset V4: Unified image classification, object detection, and visual relationship detection at scale. *arXiv:1811.00982*.

Landsiedel, C., Rieser, V., Walter, M. R., and Wollherr, D. (2017). A review of spatial reasoning and interaction for real-world robotics. *Advanced Robotics*, 31(5):222–242.

Leonard, J., How, J., Teller, S., Berger, M., Campbell, S., Fiore, G., Fletcher, L., Frazzoli, E., Huang, A., Karaman, S., Koch, O., Kuwata, Y., Moore, D., Olson, E., Peters, S., Teo, J., Truax, R., Walter, M., Barrett, D., Epstein, A., Maheloni, K., Moyer, K., Jones, T., Buckley, R., Antone, M., Galejs, R., Krishnamurthy, S., and Williams, J. (2008). A perception-driven autonomous urban vehicle. *Journal of Field Robotics*, 25(10):727–774.

Lin, T.-Y., Maire, M., Belongie, S., Hays, J., Perona, P., Ramanan, D., Dollár, P., and Zitnick, C. L. (2014). Microsoft COCO: Common objects in context. In *Proceedings of the European Conference on Computer Vision (ECCV)*, pages 740–755.

MacMahon, M., Stankiewicz, B., and Kuipers, B. (2006). Walk the talk: Connecting language, knowledge, and action in route instructions. In *Proceedings of the National Conference on Artificial Intelligence (AAAI)*, pages 1475–1482.

Maimone, M., Cheng, Y., and Matthies, L. (2007). Two years of visual odometry on the Mars exploration rovers. *Journal of Field Robotics*, 24(3):169–186.

Marshall, J., Barfoot, T., and Larsson, J. (2008). Autonomous underground tramming for center-articulated vehicles. *Journal of Field Robotics*, 25(6-7):400–421.

Martínez Mozos, O., Triebel, R., Jensfelt, P., Rottmann, A., and Burgard, W. (2007). Supervised semantic labeling of places using information extracted from sensor data. *Robotics and Autonomous Systems*, 55(5):391–402.

Matuszek, C., Fox, D., and Koscher, K. (2010). Following directions using statistical machine translation. In *Proceedings of the ACM/IEEE International Conference on Human-Robot Interaction (HRI)*, pages 251–258.

Matuszek, C., Herbst, E., Zettlemoyer, L., and Fox, D. (2012). Learning to parse natural language commands to a robot control system. In *Proceedings of the International Symposium on Experimental Robotics (ISER)*, pages 403–415.

Meger, D., Forssén, P.-E., Lai, K., Helmer, S., McCann, S., Southey, T., Baumann, M., Little, J. J., and Lowe, D. G. (2008). Curious George: An attentive semantic robot. *Robotics and Autonomous Systems*, 56(6):503–511.

Mei, H., Bansal, M., and Walter, M. R. (2016). Listen, attend, and walk: Neural mapping of navigational instructions to action sequences. In *Proceedings of the National Conference on Artificial Intelligence (AAAI)*.

Miller, I., Campbell, M., Huttenlocher, D., Kline, F.-R., Nathan, A., Lupashin, S., Catlin, J., Schimpf, B., Moran, P., Zych, N., Garcia, E., Kurdziel, M., and Fujishima, H. (2008). Team Cornell's Skynet: Robust perception and planning in an urban environment. *Journal of Field Robotics*, 25(8):493–527.

Mirowski, P., Grimes, M., Malinowski, M., Hermann, K. M., Anderson, K., Teplyashin, D., Simonyan, K., Zisserman, A., and Hadsell, R. (2018). Learning to navigate in cities without a map. In *Advances in Neural Information Processing Systems (NeurIPS)*, pages 2419–2430.

Misra, D. K., Sung, J., Lee, K., and Saxena, A. (2016). Tell me Dave: Context-sensitive grounding of natural language to manipulation instructions. *International Journal of Robotics Research*, 35(1-3):281–300.

Montemerlo, M., Becker, J., Bhat, S., Dahlkamp, H., Dolgov, D., Ettinger, S., Haehnel, D., Hilden, T., Hoffmann, G., Huhnke, B., Johnston, D., Klumpp, S., Langer, D., Levandowski, A., Levinson, J., Marcil, J., Orenstein, D., Paefgen, J., Penny, I., Petrovskaya, A., Pflueger, M., Stanek, G., Stavens, D., Vogt, A., and Thrun, S. (2008). Junior: The Stanford entry in the Urban Challenge. *Journal of Field Robotics*, 25(9):569–597.

Nagatani, K., Kiribayashi, S., Okada, Y., Otake, K., Yoshida, K., Tadokoro, S., Nishimura, T., Yoshida, T., Koyanagi, E., Fukushima, M., et al. (2013). Emergency response to the nuclear accident at the Fukushima Daiichi Nuclear Power Plants using mobile rescue robots. *Journal of Field Robotics*, 30(1):44–63.

Nagatani, K., Yoshida, K., Kiyokawa, K., Yagi, Y., Adachi, T., Saitoh, H., Suzuki, T., and Takizawa, O. (2008). Development of a networked robotic system for disaster mitigation. In *Proceedings of the International Conference on Field and Service Robotics (FSR)*, pages 453–462.

Nüchter, A., Surmann, H., Lingemann, K., and Hertzberg, J. (2003). Semantic scene analysis fo scanned 3D indoor environments. In *Proceedings of the International Workshop on Vision, Modeling and Visualization (VMV)*, pages 215–221.

Oh, J., Howard, T. M., Walter, M., Barber, D., Zhu, M., Park, S., Suppe, A., Navarro-Serment, L., Duvallet, F., Boularias, A., Romero, O., Vinokrov, J., Keegan, T., Dean, R., Lennon, C., Bodt, B., Childers, M., Shi, J., Daniilidis, K., Roy, N., Lebiere, C., Hebert, M., and Stentz, A. (2017). Integrated intelligence for human-robot teams. In *Proceedings of the International Symposium on Experimental Robotics (ISER)*, pages 309–322.

Olson, E. (2011). AprilTag: A robust and flexible visual fiducial system. In *Proceedings of the IEEE International Conference on Robotics and Automation (ICRA)*, pages 3400–3407.

Olson, E., Leonard, J., and Teller, S. (2006). Fast iterative optimization of pose graphs with poor initial estimates. In *Proceedings of the IEEE International Conference on Robotics and Automation (ICRA)*, pages 2262–2269.

Paskin, M. A. (2003). Thin junction tree filters for simultaneous localization and mapping. In *Proceedings of the International Joint Conference on Artificial Intelligence (IJCAI)*, pages 1157–1164.

Patki, S., Daniele, A., Walter, M., and Howard, T. (2019). Inferring compact representations for efficient natural language understanding of robot instructions. In *Proceedings of the IEEE International Conference on Robotics and Automation (ICRA)*, pages 6926–6933.

Patki, S., Fahnestock, E., Howard, T. M., and Walter, M. R. (2020). Language-guided semantic mapping and mobile manipulation in partially observable environments. In *Proceedings of the Conference on Robot Learning (CoRL)*, pages 1201–1210.

Patki, S. and Howard, T. M. (2018). Language-guided adaptive perception for efficient grounded communication with robotic manipulators in cluttered environments. In *Proceedings of the Annual Meeting of the Special Interest Group on Discourse and Dialogue (SIGDIAL)*, pages 151–160.

Paul, R., Arkin, J., Aksaray, D., Roy, N., and Howard, T. M. (2018). Efficient grounding of abstract spatial concepts for natural language interaction with robot platforms. *International Journal of Robotics Research*, 37(10):1269–1299.

Paul, R., Arkin, J., Roy, N., and Howard, T. M. (2016). Efficient grounding of abstract spatial concepts for natural language interaction with robot manipulators. In *Proceedings of Robotics: Science and Systems (RSS)*.

Pronobis, A. and Jensfelt, P. (2012). Large-scale semantic mapping and reasoning with heterogeneous modalities. In *Proceedings of the IEEE International Conference on Robotics and Automation (ICRA)*, pages 3515–3522.

Pronobis, A., Martínez Mozos, O., Caputo, B., and Jensfelt, P. (2010). Multi-modal semantic place classification. *International Journal of Robotics Research*, 29(2–3):298–320.

Ranganathan, A. and Dellaert, F. (2011). Online probabilistic topological mapping. *International Journal of Robotics Research*, 30(6):755–771.

Rasouli, A., Lanillos, P., Cheng, G., and Tsotsos, J. K. (2020). Attention-based active visual search for mobile robots. *Autonomous Robots*, 44(2):131–146.

Ratliff, N. D., Bagnell, J. A., and Zinkevich, M. A. (2006). Maximum margin planning. In *Proceedings of the International Conference on Machine Learning (ICML)*, pages 729–736.

Redmon, J. and Farhadi, A. (2018). YOLOv3: An incremental improvement. *arXiv:1804.02767*.

Roberts, J. M., Duff, E. S., Corke, P. I., Sikka, P., Winstanley, G. J., and Cunningham, J. (2000). Autonomous control of underground mining vehicles using reactive navigation. In *Proceedings of the IEEE International Conference on Robotics and Automation (ICRA)*, pages 3790–3795.

Ross, S., Gordon, G. J., and Bagnell, J. A. (2011). A reduction of imitation learning and structured prediction to no-regret online learning. In *Proceedings of the International Conference on Artificial Intelligence and Statistics (AISTATS)*, pages 627–635.

Roy, D., Hsiao, K.-Y., and Mavridis, N. (2003). Conversational robots: Building blocks for grounding word meaning. In *Proc. HLT-NAACL Workshop on Learning Word Meaning from Non-Linguistic Data*, pages 70–77.

Ryu, D., Kang, S., Kim, M., and Song, J.-B. (2004). Multi-modal user interface for teleoperation of ROBHAZ-DT2 field robot system. In *Proceedings of the IEEE/RSJ International Conference on Intelligent Robots and Systems (IROS)*, pages 168–173.

Sadeghi, F. and Levine, S. (2017). CAD2RL: Real single-image flight without a single real image. In *Proceedings of Robotics: Science and Systems (RSS)*.

Scheding, S., Dissanayake, G., Nebot, E. M., and Durrant-Whyte, H. (1999). An experiment in autonomous navigation of an underground mining vehicle. *IEEE Transactions on Robotics and Automation*, 15(1):85–95.

Scheding, S., Nebot, E. M., Stevens, M., Durrant-Whyte, H., Roberts, J., Corke, P., Cunningham, J., and Cook, B. (1997). Experiments in autonomous underground guidance. In *Proceedings of the IEEE International Conference on Robotics and Automation (ICRA)*, pages 1898–1903.

She, L. and Chai, J. (2017). Interactive learning of grounded verb semantics towards human-robot communication. In *Proceedings of the Association for Computational Linguistics (ACL)*, pages 1634–1644.

Shridhar, M. and Hsu, D. (2018). Interactive visual grounding of referring expressions for human-robot interaction. In *Proceedings of Robotics: Science and Systems (RSS)*.

Singh, H., Can, A., Eustice, R., Lerner, S., McPhee, N., and Roman, C. (2004). Seabed AUV offers new platform for high-resolution imaging. *Eos, Transactions American Geophysical Union*, 85(31):289–296.

Smola, A., Gretton, A., Song, L., and Schölkopf, B. (2007). A Hilbert space embedding for distributions. In *Proceedings of the International Conference on Algorithmic Learning Theory (ALT)*, pages 13–31.

Syed, U., Bowling, M., and Schapire, R. E. (2008). Apprenticeship learning using linear programming. In *Proceedings of the International Conference on Machine Learning (ICML)*, pages 1032–1039.

Tai, L., Paolo, G., and Liu, M. (2017). Virtual-to-real deep reinforcement learning: Continuous control of mobile robots for mapless navigation. In *Proceedings of the IEEE/RSJ International Conference on Intelligent Robots and Systems (IROS)*, pages 31–36.

Tellex, S., Knepper, R., Li, A., Rus, D., and Roy, N. (2014). Asking for help using inverse semantics. In *Proc. Robotics: Science and Systems (RSS)*.

Tellex, S., Kollar, T., Dickerson, S., Walter, M. R., Banerjee, A. G., Teller, S., and Roy, N. (2011). Understanding natural language commands for robotic navigation and mobile manipulation. In *Proceedings of the National Conference on Artificial Intelligence (AAAI)*, pages 1507–1514.

Tellex, S., Thaker, P., Deits, R., Kollar, T., and Roy, N. (2012). Toward information theoretic human-robot dialog. In *Proceedings of Robotics: Science and Systems (RSS)*.

Thomason, J., Sinapov, J., Mooney, R. J., and Stone, P. (2018). Guiding exploratory behaviors for multi-modal grounding of linguistic descriptions. In *Proceedings of the National Conference on Artificial Intelligence (AAAI)*, pages 5520–5527.

Thomason, J., Sinapov, J., Svetlik, M., Stone, P., and Mooney, R. J. (2016). Learning multi-modal grounded linguistic semantics by playing "I spy". In *Proceedings of the International Joint Conference on Artificial Intelligence (IJCAI)*, pages 3477–3483.

Thomason, J., Zhang, S., Mooney, R. J., and Stone, P. (2015). Learning to interpret natural language commands through human-robot dialog. In *Proceedings of the International Joint Conference on Artificial Intelligence (IJCAI)*, pages 1923–1929.

Thrun, S., Liu, Y., Koller, D., Ng, A., Ghahramani, Z., and Durrant-Whyte, H. (2004). Simultaneous localization and mapping with sparse extended information filters. *International Journal of Robotics Research*, 23(7–8):693–716.

Thrun, S., Montemerlo, M., Dahlkamp, H., Stavens, D., Aron, A., Diebel, J., Fong, P., Gale, J., Halpenny, M., Hoffmann, G., Lau, K., Oakley, C., Palatucci, M., Pratt, V., Stang, P., Strohband, S., Dupont, C., Jendrossek, L.-E., Koelen, C., Markey, C., Rummel, C., van Niekerk, J., Jensen, E., Alessandrini, P., Bradski, G., Davies, B., Ettinger, S., Kaehler, A., Nefian, A., and Mahoney, P. (2006). Stanley: The robot that won the DARPA Grand Challenge. *Journal of Field Robotics*, 23(9):661–692.

Torralba, A., Murphy, K. P., Freeman, W. T., and Rubin, M. A. (2003). Context-based vision system for place and object recognition. In *Proceedings of the International Conference on Computer Vision (ICCV)*, pages 273–280.

Tucker, M., Aksaray, D., Paul, R., Stein, G. J., and Roy, N. (2017). Learning unknown groundings for natural language interaction with mobile robots. In *International Symposium on Robotics Research (ISRR)*, pages 317–333.

Urmson, C., Anhalt, J., Bagnell, D., Baker, C., Bittner, R., Clark, M. N., Dolan, J., Duggins, D., Galatali, T., Geyer, C., Gittleman, M., Harbaugh, S., Hebert, M., Howard, T. M., Kolski, S., Kelly, A., Likhachev, M., McNaughton, M., Miller, N., Peterson, K., Pilnick, B., Rajkumar, R., Rybski, P., Salesky, B., Seo,

Y.-W., Singh, S., Snider, J., Stentz, A., Whittaker, W. R., Wolkowicki, Z., Ziglar, J., Bae, H., Brown, T., Demitrish, D., Litkouhi, B., Nickolaou, J., Sadekar, V., Zhang, W., Struble, J., Taylor, M., Darms, M., and Ferguson, D. (2008). Autonomous driving in urban environments: Boss and the Urban Challenge. *Journal of Field Robotics*, 25(8):425–466.

Urmson, C., Ragusa, C., Ray, D., Anhalt, J., Bartz, D., Galatali, T., Gutierrez, A., Johnston, J., Harbaugh, S., "Yu" Kato, H., Messner, W., Miller, N., Peterson, K., Smith, B., Snider, J., Spiker, S., Ziglar, J., "Red" Whittaker, W., Clark, M., Koon, P., Mosher, A., and Struble, J. (2006). A robust approach to high-speed navigation for unrehearsed desert terrain. *Journal of Field Robotics*, 23(8):467–508.

Vasudevan, S. and Siegwart, R. (2008). Bayesian space conceptualization and place classification for semantic maps in mobile robotics. *Robotics and Autonomous Systems*, 56(6):522–537.

Walter, M. R., Antone, M., Chuangsuwanich, E., Correa, A., Davis, R., Fletcher, L., Frazzoli, E., Friedman, Y., Glass, J., How, J. P., Jeon, J. H., Karaman, S., Luders, B., Roy, N., Tellex, S., and Teller, S. (2015). A situationally-aware voice-commandable robotic forklift working alongside people in unstructured outdoor environments. *Journal of Field Robotics*, 32(4):590–628.

Walter, M. R., Eustice, R. M., and Leonard, J. J. (2007). Exactly sparse extended information filters for feature-based SLAM. *International Journal of Robotics Research*, 26(4):335–359.

Walter, M. R., Hemachandra, S., Homberg, B., Tellex, S., and Teller, S. (2013). Learning semantic maps from natural language descriptions. In *Proceedings of Robotics: Science and Systems (RSS)*.

Walter, M. R., Hemachandra, S., Homberg, B., Tellex, S., and Teller, S. (2014). A framework for learning semantic maps from grounded natural language descriptions. *International Journal of Robotics Research*, 33(9):1167–1190.

Williams, S. B., Pizarro, O. R., Jakuba, M. V., Johnson, C. R., Barrett, N. S., Babcock, R. C., Kendrick, G. A., Steinberg, P. D., Heyward, A. J., Doherty, P. J., et al. (2012). Monitoring of benthic reference sites: using an autonomous underwater vehicle. *IEEE Robotics & Automation Magazine*, 19(1):73–84.

Winograd, T. (1971). *Procedures As A Representation for Data in a Computer Program for Understanding Natural Language*. PhD thesis, Massachusetts Institute of Technology.

Yamauchi, B. M. (2004). PackBot: A versatile platform for military robotics. In *Proceedings of the International Society for Optics and Photonics (SPIE), Unmanned Ground Vehicle Technology VI*, volume 5422, pages 228–237.

Yoerger, D. R., Jakuba, M., Bradley, A. M., and Bingham, B. (2007). Techniques for deep sea near bottom survey using an autonomous underwater vehicle. *The International Journal of Robotics Research*, 26(1):41–54.

Zender, H., Martínez Mozos, O., Jensfelt, P., Kruijff, G., and Burgard, W. (2008). Conceptual spatial representations for indoor mobile robots. *Robotics and Autonomous Systems*, 56(6):493–502.

Zeng, W., Luo, W., Suo, S., Sadat, A., Yang, B., Casas, S., and Urtasun, R. (2019). End-to-end interpretable neural motion planner. In *Proceedings of the IEEE Conference on Computer Vision and Pattern Recognition (CVPR)*, pages 8660–8669.

Zhu, Y., Mottaghi, R., Kolve, E., Lim, J. J., Gupta, A., Fei-Fei, L., and Farhadi, A. (2017). Target-driven visual navigation in indoor scenes using deep reinforcement learning. In *Proceedings of the IEEE International Conference on Robotics and Automation (ICRA)*, pages 3357–3364.